POLITECNICO DI TORINO

**Corso di Laurea Magistrale in Ingegneria Energetica e Nucleare**

Tesi di Laurea Magistrale

# Adsorption CFD model of alginate-based atmospheric water harvesting system

**Relatore:**
Prof. Marco Simonetti
**Correlatore**:
Ing. Vincenzo Maria Gentile

**Candidato:**

Beatrice Fenu

Anno Accademico 2019-2020

*Abstract*

*Inadequate water supply is one of the most crucial issue to laid down as a priority. Water demand increases worldwide by 1% per year, due to a combination of population growth, economic development, production of energy and human consumption habits, associated with climate change. Therefore, it becomes necessary to find new water resources for meeting the increasing demand. The possibility to extract water from air gives attention to the development of atmospheric water harvesting technologies, in particular that one based on adsorption materials.*

*This work aims to study the behaviour of alginate-based sorption material in an atmospheric water extraction system. The adsorption process is simulated by a Computational Fluid Dynamics model, performed by the software STAR CCM+. The model is able to simulate the system, adapting to a chosen configuration through geometric corrections and by entering specific sorbent material properties. In particular, hexagonal-shape configuration is chosen in order to improve the efficiency of the system. Both regeneration and adsorption phase are investigated in order to evaluate the performances of the system during a complete cycle of adsorption/desorption.*

*The CFD model results are compared to experimental data obtained by testing an hexagonal-shape adsorption heat exchanger coupled with alginate sorbent. The study is oriented toward the investigation of the suitability of alginate and its excellent properties that promote the adsorption of water from atmospheric air.*

# Summary

# Introduction

One of the most discussed global problem is water scarcity that affects around four billion people in different counties for at least one month in a year, including a half billion of people affected for the entire year. For this reason the water management becomes a thematic of interest in the innovation energy technology contest.

Water demand increases worldwide by 1% per year since the 1980s[1], due to a combination of different aspects such as population growth, economic development, production of energy and human consumption habits. Increasingly outward-looking of water demand are expected until 2050, driven by the rising demand in all major use sectors, in particular the industrial and domestic sectors. As reported in UNWWD Report 2019, the estimation of future global agriculture consumption of water sees an increase of 20% until 2050, or higher if efficiency of agricultural production will not improve. This because much of the need of water for irrigation will be in regions already suffering from water scarcity. Most energy sources require water in production process, like extraction of raw material, cooling phase in thermal processes and cleaning processes powering turbines to generate hydroelectricity. For that processes, global energy consumption is estimated to increase by 50% until 2035. As regard industrial process, the increase of water demand results from the increase of economic activity. This aspect carries consumption habit to modify. Most of water source demand comes from urban centre requiring drinking water, sanitation and drainage. The urban population of the world continuously grows up by birth rate growth and net migration from countryside to city: nowadays the 55% of the population lives in urban areas and it is expected to grow up to 65% in 2050 (UNDESA 2014[2]). In this case the water demand is satisfied principally by the extraction from the available sources in groundwater or dam.

Another issue water scarcity faces up is global climate change that influences ecosystem and livelihood of societies. Predictably global climate change will affect the availability of water because of alteration of the main resource and atmospheric events like rainfall distribution, soil moisture, glacier melt, river and groundwater flows. The water-related

linkage between seemingly different trends is the relationship between rapid urbanization, increased vulnerability to climate changes causing floods and droughts, and the increased risk of displacement. However, in terms of both the number of people affected and the number of people killed, the impacts of floods, droughts and conflicts are totally outweighed by the number of those affected or killed by inadequate drinking water and sanitation services (Figure 1).

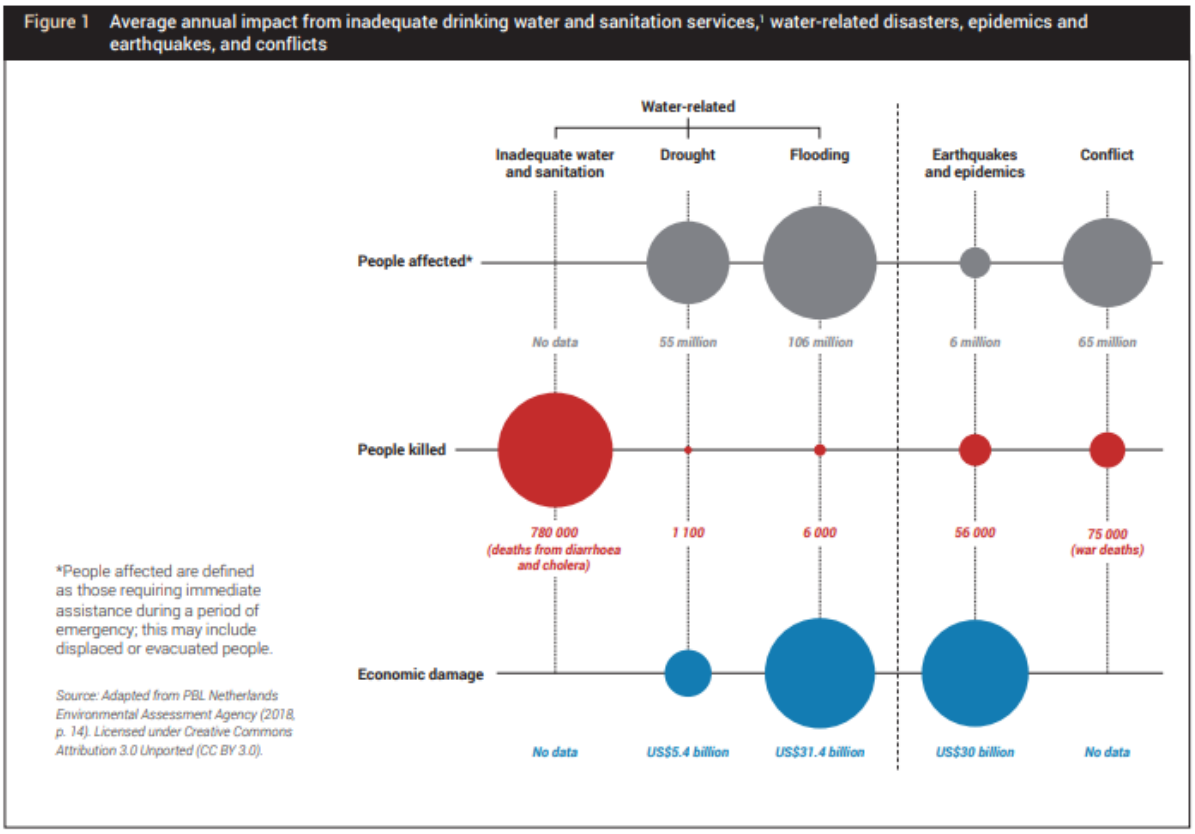


**Figure 1. Average annual impact from inadequate drinking water and sanitation services**

The water theme involves all aspects of development and for this reason it is a key element in global climate crises, for which the solution reside in the improvement of water demand management, that means to find new resources to guarantee fresh and sustainable water for human consumption and better to use standard resources like recycling of wastewater for industrial purposes [3]. Flexible and integrated clean water production systems are required, to allocate water where it is most needed. This requires appropriately defined water rights, an topic which is insufficiently considered in many regions. Water policies need to place quality and quantity problems on an equal footing.

Innovative techniques and business models will be needed, to secure water-related services, while the consumes of water, energy or capital decrease. In particular, the private sector will be an important player to change the habit in the prospective of low water consumption as personal commitment. Public policies must support the development and diffusion of such innovations, including in developing countries.

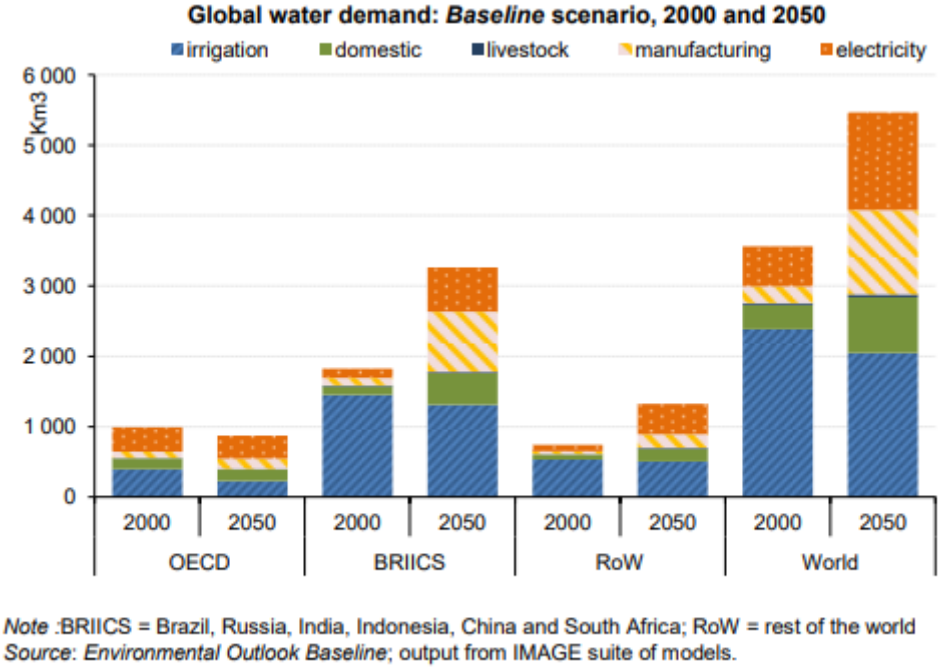


**Figure 2 Global water demand: Baseline scenario, 2000 and 2050. Source: OECD (2012a)**

The aim of this work is to present a CFD model that describes the operations of an adsorbent heat exchanger, in order to validate its feasibility with different configurations and different materials. In particular honeycomb structured alginate-based heat exchanger is considered and its performances are compared to experimental data.

# Chapter 1

# Atmospheric water harvesting

Atmospheric water is nowadays considered a renewable reservoir of water and the way to harvest it has to be studied more in deep. The water extracted has normally such a good quality that it can be considered potable and adapted for domestic use and agricultural purpose.

The main innovative technologies for potable water production can be resumed as follow:

- Desalination of sea water (by reverse osmosis (RO))
- Atmospheric water harvesting
- Rainwater harvesting
- Recycled and cleaned wastewater from industrial processes

The most studied and applied technologies concerns desalination and atmospheric water extraction.

Desalination of sea water is one of the most promising technologies for intensive production of fresh water. The principal idea is extract fresh water from seawater, and there are several method to do that, divided into membrane-based and thermal-based method. In general all methods require large amount of saline water and they are limited to these regions that have free access to sea water. Moreover, desalination systems have to be supported by high investment cost and operation cost when piping and pumping infrastructure are requested [4]. Such an outlay may be cost prohibitive, especially when the water should be delivered to dispersed areas.

Water harvesting from air becomes one of the promising source of water supplying for community use in arid and decentralized areas. On one hand the need to have cleaned water concerns around 1.7 billion people per year living in low sanitation condition [5], on the other hand the accessibility to fresh water helps the economic development in deserted areas, where traditional sources of water are not available.

Atmospheric water harvesting technologies, according to the existing airborne forms of water, can be in three main types: clouds collection, fog collection, and water vapour

collection from the air. This distinction is made comparing the size of rain drop that is about 0.5-5mm of diameter to those of cloud and fog, that are made up of smaller drop whose size diameter is 1-40 μm, and comparing the concentration of water, bigger in fog and clouds.
In general, applications for dew point water collection and fog collection require high relative humidity, usually around 50%, conditions that are typical of those regions where fresh water can be collected from other resources, e. g. lakes, rivers or ocean. In the following discussion applications able to harvest water from air at lower relative humidity are presented.

## 1.1 Fog harvesting

Fog collection is a technology relevant in arid coastal zone, like South America coast (Chile and Peru), West Africa (Namibia) and Middle East (Saudi Arabia, Oman). The most known method to collect fog water is traps droplets carried by the wind placing a mesh perpendicular to the wind motion. After, the droplets coalesce until they are heavy enough to fall by gravity force and then they are transported to a tank. Typical conditions that characterized fog and the common system of collection with an efficiency of 50% are liquid water content of fog around 0.1-0.5 $g/m^3$ and 3 m/s wind speed. The advanced systems are able to produce 3-7 $kg/day/m^2$ of water [6]. This type of system has some drawbacks that regard the economic aspect and the availability near the residential areas. Collectors are not always assembled near urban centre and that implies the installation of pipelines to make the water residentially available. This configuration requires high installation costs and make the systems uneconomic and hydraulically difficult. To overcome these technical problems, Schemenauer and Cereda [7] list the major aspects a fog collection system should have to be convenient:

- installation where fog is a frequent weather event,
- high liquid water content fog,
- fog collection must be coupled with wind to achieve higher efficiency.

Another point to focus on is the efficiency of collection that depends on mesh shape that has to be not too coarse or too fine. A solution can be “fog harps” to replace traditional cross-like mesh or spider-web-like mashes assembled by low-cost cavity-microfibers in directional water transportation. These studies have potential for improvement but they are conducted

under controlled laboratory conditions and need development to verify their true performance in environmental conditions.


**Figure 3. Example of fog harvesting system in South America**

## 1.2 Dew water collection

Compared to fog collection, dew water collection has been recognized as a good candidate for collecting water because it is low influenced by climatic and geographical conditions. It is also a cheaper solution than cloud seeding. Initially, the system was based on passive condenser, that means no extra energy input. The International Organization for Dew Utilization has standardized the main characteristic of a dew collection system in term of methodology, instrument, environment of experimental tests. The recommended material is a low-density polyethylene (PE) because of its hydrophilic properties that favour dew formation: the nucleation barrier at the start of condensation phase is lower and the emissivity near infrared is higher. In arid climates the maximum yield of dew water is typically 0.3-0.6 kg/day/$m^2$ in comparison with the ability of condenser to collect the radiative cooling available, around 0.8 kg/day/$m^2$. The process has limits as regards the rate of radiative heat exchange, the surface of heat exchange and the weather condition because the ratio of latent to sensible heat exchanged between the surface and the air depends on the weather. Another innovative technology for dew collection in areas with quality and quantity water problem can be active condensers. They work similar to dehumidifier and are more effective than passive condenser in term of water yield per day, but they require a

source of energy for operations which makes operating cost higher. Recent researches are centred in making active condenser design in a way that they can minimize the energy required using renewable energy sources integrated into the condenser. The water yield of active condenser varies depending on the design: 20-200 kg/day [8].

In general, for climatic regions characterized by high temperature and relative humidity typical of costal weather conditions, cooling and dehumidification processes can be suitable solutions for the production of fresh water if they are optimized by coupling a solar-powered system. In fact, to reduce the cost energy produced by fossil fuel, the solar energy is the most feasible resource, because of its availability in that regions. Solar photovoltaic (PV)-powered thermoelectric condensers could be a solution due to their small volume and relative low cost.

Two main methods for water harvesting from air driven by solar radiation are presented:

sorption-regeneration-condensation method

dew water harvesting by solar powered sorption chiller. [9]

### 1.2.1 Sorption-regeneration-condensation method

The first method uses sorption material like desiccants to subtract the moisture contained in the air and then desorbs the water out. Afterwards the material is regenerated for further cycles and the extracted water is condensed at ambient temperature. Usually water is taken up during night because the relative humidity is higher and, thanks to a difference in pressure between desiccant and moisture, mass transfer happens from atmosphere to absorbent. The resulting absorbent is diluted. Then water is desorbed from desiccant during daytime thanks to the heat provided by the solar radiation. The resulting heated water vapour evaporated from the solution meets a colder surface and it is brought under its dew point, condensing in ambient conditions. The fact that sees the ambient air used as a coolant implies the maintenance of a sufficient air stream able to reject the heat of condensation. The performance of a system during night depends on the mass transfer potential [10].

In figure 4, some example system of sorption-regeneration-condensation are shown: two cases refer to a solar still, that is a glass-covered house with desiccant inside. At night the window is open and the desiccant absorbs the moisture in the air by natural or forced convection. During daytime the incident solar radiation hits the desiccant and it is absorbed, resulting in desiccant temperature increase. The release water vapour is condensed

underneath the glass coverage (case A) or in a condenser powered by ambient cooling (case B). The third case describes a sandwich plate composed by a first metal plate, which is composed by solar absorber in one side and desiccant on the other side, and another plate that acts as a condenser. These types of AWGs are considered as passive systems characterized by a water productivity in the range of 1-2.5 kg/day/m$^2$ of collector area. An active AWG system is shown in figure D which is composed by a compact active sorber with more complex structure because it needs solar collector system independent from the desiccant and an additional condenser.

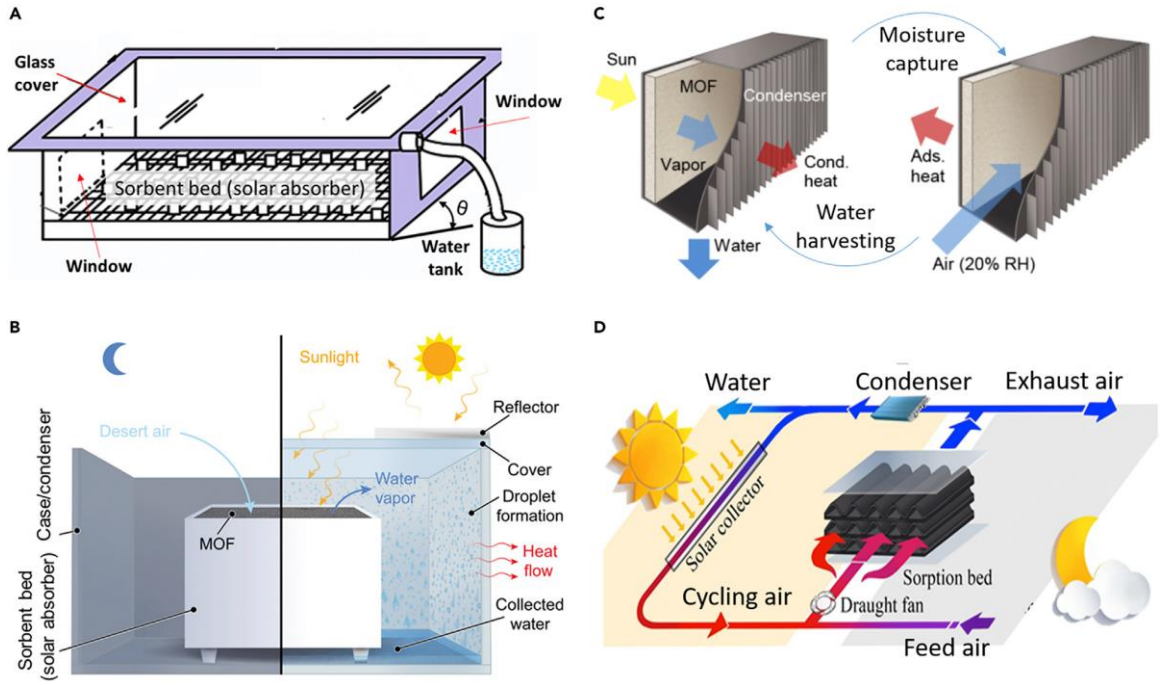


**Figure 4. Sorption regeneration condensation system, several applied configurations [5]**

To resume, the necessity of water production in arid zones meets the possibility to realize solar desiccant systems. Even if the feasibility of this technology for that kind of climate, the economic aspect limits the utilization of the units in large scale [10]. In the following, solutions regarding new ideas to improve the economic aspect are described. In particular the adjustments are related to the type of the desiccant, to the implementation of the efficiency of coupled solar system with extraction system and to the investigation of new glass shapes, covering desiccant beds.

In desert region, a smart solution to reduce the cost of desiccant bed is the desiccant mixed with sandy layer of ground surface. In this way the cost of vapour absorption is minimized [11].

In ambient condition, the desiccant and the sandy layer are mixed to absorb water vapour in the night. The layer is covered with a greenhouse where the desiccant is regenerated during day and water vapour can condense because the cold surface of the greenhouse. The rate of water production can be estimated by the design parameters of the absorption bed, affected by the ratio of mass between desiccant and sand

Another solution can be the use of sandy bad solar collector system in which the sandy bad is impregnated with 30% concentration of calcium chloride. This kind of systems produce 1.2 l of fresh water per unit surface of glass cover per day

Application of solar concentrator for the production of potable water sees an improvement in the extraction process of water, as described by AQUASOLIS project [12]. The capability of solar concentration plants of producing heat at temperatures over 150° permits to investigate the use of solar energy for water purification by distillation and, at the same time, the high temperature fluid generated by the plant can be used to drive adsorption chillers that can extract water from the atmosphere

Glass pyramid shape with a multi-shelf solar system to extract water from humid air is

explored: the pyramid sides are opened during night to permit the moist air to saturate the desiccant bed, and they are closed during the day to extract the moisture by solar radiation. Sometime two pyramid are applied with different type of bed material. This kind of system is experimentally studied at different climatic conditions to know the effect on absorption and regeneration processes. The typical water production is about 2.5 *l*/(day m2)

The most effective improvement both in term of efficiency of sorption process and economic aspect could be the application of new material like for instance selective composite adsorbent. This argument is developed in chapter 2.

### 1.2.2 Dew water harvesting by solar power sorption chillers

Typical atmospheric water generators utilise refrigeration to cool large volumes of air below the dew point to condense water [13]. Contrary to the first method, dew water harvesting by sorption chiller can work continuously during day thanks to the integration of an heat

storage system. This technology is driven by direct cooling that means the refrigeration cycle is based on heat pump or an absorption chiller. Ambient air, needed in large quantity, can be cooled below its dew point and the obtained condensed liquid water is collected. Low temperature at the condenser is required, especially in region characterized by a low relative humidity condition. So, the heat sink for the condensation consumes energy to maintain a difference of temperature between ambient and condenser unit. In addition the heat of condensation of the collected water has to be discharged. The amount of energy consumed to collect water from the air dramatically increases as the humidity or ambient temperature decreases. Due to the low humidity, the dew point temperature in arid regions is less than 15 °C, even below 0 °C in extremely dry desert climate. As a result, this method is infeasible for the huge energy consumption owed to reduce air temperature below dew point. In addition during refrigeration the frost could occur and act as insulator reducing airflow and making the process inefficient. A way to face up these problem is to install more photovoltaic or solar panel but high costs of installation and maintenance make this solution economically inconvenient [14].

## 1.3 Consideration about AWGs

Summarizing, technologies of AWGs are presented in Table 1. They can be presented in three main categories: direct harvesting by condensation, vapour concentration by membrane or desiccant, by-product collection from an integrated system. Selection of methods is an engineering decision depending on both local climatic conditions and economic factors such as capital, operation, and energy costs.

**Table 2. Summary of AWGs [5]**

| Methods | Features | Capacity | Problems | Alternatives | Challenges | Applications |
|---|---|---|---|---|---|---|
| **Fog mesh** | Easy to construct | 1.5–12 kg/day/m2 | limited to locations | nano-engineering mesh surface | low collection efficiency | mount by the sea |
| **Radiative dew collector** | passive way | collector 0.3–0.6 kg/day/m2 | large heat loss | high-performance emitter | metamaterials | low-T water production |
| **Electric chiller Sorption** | high output compact | 0.25 Wh/g (electricity) | great latent load | DEHP | durability and reliability | potable water production |

| | | | | | | |
|---|---|---|---|---|---|---|
| **chiller** | | | | | | |
| **Sorption-based AWG (solar distiller)** | ambient cooling | 1.0–2.5 kg/day/m2 | high Tcond | water-cooling condenser | Heat transfer enhancement | scalable water supply |
| **Sorption-based AWG (solar air heating)** | active condenser | 2.0 kWh/kg (heat) | large heat loss | solar water-heating sorber | pump | scalable water supply |
| **Sorption-based AWG (sandwich plate)** | air cooling | 1.2 kg/day/m2 | thickness of desiccant layer | high k desiccant | desiccant | electronic cooling |
| **TEC dew collector (solar PV driven)** | small &compact | COP < 0.1 | low energy efficiency | desiccant-enhanced heat sink | proper application | meet minimum water load |
| **Integrated system** | by-product | depends on the latent load | cooling dependence | NA | NA | offsetting water use of A/C |

*AWG, atmospheric water generator; COP, coefficient of performance; DEHP, desiccant-enhanced heat pump; DRH, deliquescence relative humidity; MHI, Moisture Harvesting Index; RH, relative humidity; RR, recovery ratio of the feed air; SEC, specific energy consumption; SWP, specific water productivity; PCM, phase change material*.

Several improvements have been proposed in the literature to develop the performance of the water-harvesting system, regarding different weather conditions, materials, or collector design. However, the traditional AWGs have been restricted to small-scale water production and emergency water supply, far away to energy-efficient functions.

Some parameters that can evaluate the goodness of passive and active AWGs' system are the specific water production per day per unit collector area (SWP), the specific energy consumption per unit mass water production (SEC) and the recovery ratio for the feed air (RR) [14] .

Considering desiccant working under the conditions of ad/desorption $(T_{ad}, p_{ad}), (T_{de}, p_{de})$, the water harvesting capacity per unit mass is:

$$\Delta x = x_{ad}(T_{ad}, RP_{ad}) - x_{de}(T_{de}, RP_{de})$$

where $x_{ad}(T_{ad}, RP_{ad})$ and $x_{de}(T_{de}, RP_{de})$ are the isothermal adsorption curve. RP is the relative pressure of the water vapour, surrounding the desiccant, defined as:

$RP = \frac{p_v}{p_{sat(T_{sorber})}}$.

For the adsorption process, the $T_{ad}$ is nearly equal to the bulk temperature of air due to low kinetic, so $RP_{ad}$ can be considered equal to the relative humidity of the bulk air. For the desorption process a low $RP_{de}$ and a high $T_{de}$ are expected: lower $RP_{de}$ and higher $T_{de}$ can be obtained if the desiccant is heated by the regeneration air, with more effective heat exchange. The sorber moisture harvesting capacity in a cycle is:

$$M_{moisture} = \rho_{moisture} V_{moisture} \cdot \Delta x$$
$$= \rho_{air,sorber} Q_{air,sorber} t_{air,sorber} \cdot (d_{sorber,i} - d_{sorber,0})$$
$$= \rho_{air,desorber} Q_{air,desorber} t_{air,desorber} \cdot (d_{desorber,0} - d_{desorber,i})$$

This relation describe the desiccant's moisture harvesting capacity as a function of the regeneration temperature. Considering that the water uptake of the desiccant usually depends on the relative pressure RP, the sorber becomes a moisture adsorber during night and a desorber during daytime.

The system water harvesting capacity is defined as:

$$M_{water} = \rho_{air,sorber}\, Q_{air,sorber}\, t_{sorber} (d_{desorber,0} - d_{cond})$$

where $t_{sorber}$ is the duration of adsorption process (different from the duration of desorption process), d is the moisture content, $d_{cond}$ is the saturated humidity ratio at condensing temperature. Now the moisture recovery ratio is defined assuming the duration of adsorption and desorption are the same:

$$RR = \frac{M_{water}}{\rho_{air,sorber} Q_{air,sorber}\, t_{air,sorber}\, d_{sorber,i}} = \frac{d_{desorber,0} - d_{cond}}{d_{sorber,i}}$$

The input heat needed to warm up the regeneration air is the total heat load associated with the temperature change of the moist air, defined as:

$$W_{heat} = c_p \rho_{air,desorber}\, Q_{air,desorber}\, t_{desorber} (T_{desorber,i} - T_{ambient})$$

The specific energy consumption (SEC) when the desiccant is heated by the regeneration air is:

$$SEC = \frac{W_{heat}}{M_{water}} = c_p \cdot \frac{T_{desorber,i} - T_{ambient}}{d_{desorber,0} - d_{cond}}$$

The definition of SEC and RR indicates that optimal condition are achieved when $d_{cond}$, that depends on the condensation temperature, is low and the moisture content is high.

RR and SEC are two key parameters to characterize the performance of AWG system. To make a comment on the systems presented in the table1 related to the specific water production and to the index presented, it is possible to say that fog water collection is an efficient system but limited to a specific location with characteristic climate conditions. The passive radiative collector and the passive sorption-based AWG have low SWP due to low radiative cooling capacity and low RR, respectively. The case of solar power sorption-based AWGs with active condenser reveal great potential for efficient operation and more compact system, but they have low SEC. So, practical applications of these kind of system need to surmounted several hurdles improving thermodynamic performances of system units. Some advices are:

- Proper design to reduce heat loss or to achieve heat recovery before and after condensation process
- Cost-effective heat sink to maximize the SWP
- Energy efficiency of desiccant desorb
- Know the kinetics in term of material selection and sorber design

For sorption-based AWGs, a detailed study can relate the choice of adsorption materials, in order to improve the process.

# Chapter 2

# Adsorption materials

Solar sorption-based water harvesting systems are thought to be efficient and viable even in low RH conditions, so the selection of solid sorbent is a very important issue. In general, selective water sorbent materials have to be able to extract and release water with minimum energy request and have to be powered by renewable energy sources, like solar energy. The selection of solid sorbents relates the type of material, its shape and step position of the isotherm, saturation capacity and binding energy [15]. Porous materials such as silica gel, zeolites ACF and MOF can harvest water from atmospheric air by the adsorption process over a large range of humidity. The principal materials used as desiccant are presented above.

## 2.1 State of art of adsorption materials

Different materials are investigated in literature as sorption material. It is possible to categorize them as follow:

- ACF + salt combination
- Silica-based sorbent
- MOF
- Zeolites

### 2.1.1 ACF

Sorption/desorption process performances are improved by the application of porous matrix materials, like expanded natural graphite, silica gel, activated carbon fiber (ACF) [16].
ACFs are based on powdered activated carbon and granular activated carbon and are used mostly for water and air purification, and more recently for solvent recovery like ammonia

refrigerant [17]. They are characterized by high porosity and high surface area of 1380 $m^2/g$. Micropores are uniformly distributed inside the fiber with a pore size in the range of 0.1 to 2.0 nm and "this microstructure is the real reason to form a strong capillary force to adsorb water vapor after it used as the matrix for the salt".

In adsorption system, ACF matrix can be combined with salts like CaCl2. In the first case the composite is characterized by a water uptake of 1.7 g/g, but after adsorption the material becomes soft therefor unusable because it cannot maintain stable structure necessary for heat and mass transfer channel.

To solve this issue the research goes to composites solid sorbent with optimal structure design, high cycle sorption quantity and low desorption temperature. For example he use of LiCl shows a water uptake of 0.65 g/g at 77°C and 20% RH [18].

### 2.1.2 Silica-based sorbent

Silica gel is a synthetic and amorphous material, whose is composed by silica and oxygen in the form $SiO_2$ (silicon dioxide). The size and the packing grade of silica determine the active surface area and the pores' dimension of the material. Its framework is irregular and the porous structure is of the order of nanometres that varies from 2nm and 20nm. This structure is responsible for a huge surface area of 500-800 $m^2/g$,[19] that allows to collect water from atmospheric air moisture. Compared with other desiccant, the silica gel has high adsorption capacity of water, nearly 400 g/kg, at vapour pressure close to saturation.

In several context, silica gel is chosen as the adsorbent-adsorbate pair. This because it can be regenerated at relatively low temperature and it is widely available on the market. One of the main application of silica gel in adsorption system is the two-bed silica gel water adsorption chiller. Lot of experiments show the system works at different condition with the aim of improving the efficiency of the chiller: usually operating temperature range is between 50°C and 90°C and the obtained COP values are in the range of 0.4-0.6. For example Boelman et al [20]present a system that operates with a hot temperature of 50°C and cool temperature of 20°C obtaining a COP of 0.4. [21]

Other applications see the silica gel impregnated with CaCl2 used as adsorbent or as matrix of the composite with sodium-sulphate, synthesized by sol–gel method. [22]

### 2.1.3 MOF

Metal-organic frameworks (MOFs) are microporous crystalline materials, composed by metal ions or metal-oxygen cluster connected with organic linkers.

They are particularly attractive as sorbent material because it is demonstrated they are able to capture more water and require lower regeneration temperatures for its release compared to conventional sorbents (e.g., zeolites/silica gels or liquid brines) [23]. Moreover MOFs are sensitive to changes in temperature and in relative humidity RH, that leads large variations in water uptake and release.. Their adsorption equilibrium is characterized by step-wise isotherms and make them promising adsorbents in water harvesting systems.

The main applications for MOFs are gas storage, catalysis, heat pump and dehumidification [24]. Their high porosity and large active surface are with the flexibility with which MOFs can be modified at molecular level, make them ideally suited for the applications mentioned above and for water harvesting by adsorption process. Moreover, MOFs presents feasibility for regeneration process driven by low-grade energy sources, in particular solar energy that is abundant in arid regions with low RH. The heat given by the solar radiation is directly used for desorption and adsorption happens during the cooler night, so sorption-regeneration-condensation system are preferred in comparison with a refrigeration-based dew water system because the amount of water collected by the MOF during adsorption is much greater in the former system. Current MOFs improve their characteristics towards application in RH<20% conditions [25]: in a temperature range between 25°C and 65°C they can harvest over 0.25 L/kg of water.

Another application that sees MOF as suitable adsorbent for arid climate is the air-cooled MOF-801-based water harvesting device operating in southwestern United States, with a RH<10%. [26]

In conclusion, MOFs present several advantages like good performance driven by aggregation of water into clusters, high stability and recycling, low cost and good availability.

### 2.1.4 Zeolites

Zeolites are microporous solids, whose structure is featured by enormous amount of internal void spaces. On the chemical viewpoint, zeolites are crystalline hydrated aluminosilicates,

with three-dimensional framework. Their crystal framework is based on a network of $[AlO_4]^5$ and $[SiO_4]^{4+}$ tetrahedra where all four oxygens are being shared by adjacent tetrahedra, forming then complex unities as cages or rings. Excess of negative charge in $[AlO_4]^{5-}$ must be balanced with cationic presence; feature this that allows this class of materials the capacity to exchange cations. More than 180 different mineral species of zeolites can be distinguished, including both from natural and synthetic origin. Adsorption properties can be adjusted by varying the composition, in particular the Si/Al index (Thompson, 1998): as this ratio gets lower the zeolite's hydrofilic properties will be increased. It's also remarkable the property common to the most zeolites to be dehydrated and rehydrated without any change in volume.

The surface of these structures is basically composed by the oxygen atoms (since Si and Al are located at the center of tetrahedra). For this reason zeolites interaction with gases is mainly depending on Van Der Waals forces acting between oxygen atoms and the molecule of the gas itself. [27]

## 2.2 Alginate-based adsorption material

Sodium alginate is a hydrophilic biopolymer obtained from brown seaweeds [28]. Thanks to its incredible properties, the alginate polymer is a promising material in various industrial fields, like food, pharmaceutic and cosmetic industries that sees its main application in thickening, gel forming and colloidal stabilizing agent. The alginate can be obtained by different type of brown algae, varying its chemical structure and as consequence its properties.

In particular they are anionic structural polysaccharide, which vary in overall molecular weight and relative ratios of the (1-4)-linked β-D-mannuronate (M) and its C-5 epimer α-L-guluronate (G) residues that make up the copolymer [29]. Alginate gels strength depends on the type of ion and on the ionic binding property of the alginate. The most applied gelling cation is $Ca^{2+}$ because of it is not toxic and provides relatively strong interactions between polymer chain. Usually it is preferred to $Ba^{2+}$ for the motivation explained above structure [30]. The material obtained is water insoluble and make possible the encapsulation of macro and micro molecules. In fact, in hydration of salt for water harvesting system the sodium alginic acid play a central role as basis for the matrix of salt encapsulation: $CaCl_2$ has excellent water sorption properties, nearly 95% of its own weight, but faces up to particle

agglomeration problem which reduce gas permeability. To prevent agglomeration the salt is distributed within alginate-based matrix, improving also the water uptake by composite [31].

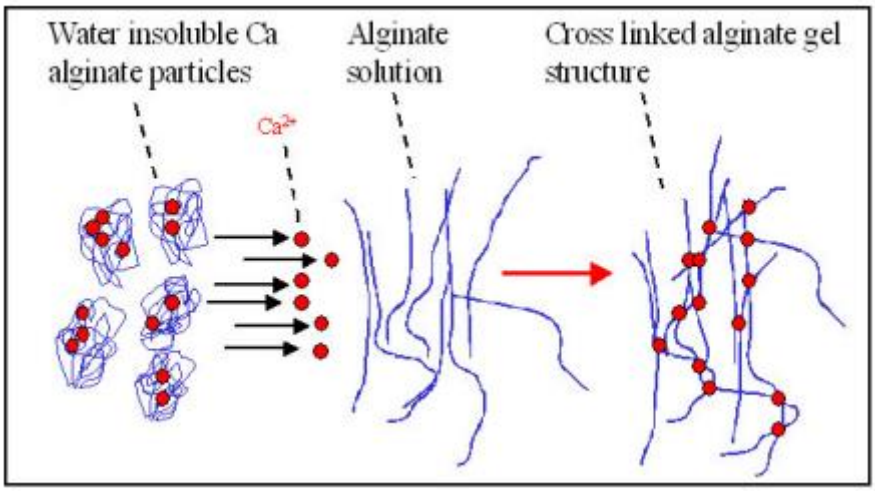


**Figure 5 Principle of delayed gelling of a hydrogel made from alginate** [32]

The main characteristic of the alginate is the capacity of adsorbing up to 200-300 times its mass in water and up to 60% of its mass in salt. These adsorbing property makes the alginate particularly interesting in its application as adsorbent material. The state of the art of alginate-based adsorbent shows its use in many functions as: porous membrane adsorbent composed by alginate and sodium in order to perform Cr(III) ions removal[33] ; water resistant sodium alginate films improved by treatment with $CaCl_2$ solution [34]; cross-linked activated organo-bentonite (AOBent) in reaction with sodium alginate and HCl to produce a low cost composite in order to act removal of cationic and anionic dye from aqueous solution [35].

Other interesting property is that alginate is a clean and eco-friendly material.

In this work an alginate-based adsorbent with 10% of $CaCl_2$ is considered.

# Chapter 3
# Adsorption model

Adsorption is one of the most interesting applied techniques for atmospheric water harvesting. It is important to investigate adsorption mechanism and performances through a deep comprehension of adsorption thermodynamic and kinetic aspects.

From the kinetic analysis of adsorption process the performances of flow-through system are determined, namely the rate of water uptake of the material may be establish [36].

In the following chapter, the adsorption model is presented in order to simulate adsorption/desorption process of an alginate-based heat exchanger.

The adsorption phenomenon as concern heat transfer and mass transfer is described by a CFD model that simulates the process inside an heat exchanger. The model is thought to suit different configurations in term of geometry setting and of material properties. It is defined by a set of theoretical equations in the way to describe heat transfer and water adsorption from air in the adsorbent material.

The software STAR-CCM+ is used to implement the adsorption process. Since no default physics of the software is conceived to simulate the adsorption, nor to do it with low computational cost, the set of equation necessary to describe the process is implemented as *Field Function*. Field Function tool allows to access field scalar or vector, solving the functions for each cell, for each iteration. In this way the physics phenomena can be completely defined, avoiding high computational costs.

The generic configuration is made of several hexagonal-shape channel where air flows with an inlet velocity and inlet temperature. The adsorption happens on the surface of the hexagonal channel and the water captured diffuses through the adsorbent material.

To develop a consistent model the following main assumptions are made:

- Comparing the diffusion of water vapour through pores of the adsorbent material with the adsorption process on its surface we can say the latter is significantly faster.

So it is possible to neglect the diffusion phenomena and to consider that a quasi-instantaneous thermodynamic equilibrium occurs on the adsorbent surface.

- The heat generated by the adsorption is considered located on the surface of the adsorbent. It is supposed to be a constant and equal to vaporization heat of water (*Hads* = 2500 *kJ/kg*).

The following set of equations allows to evaluate the water mass flux between the air and the adsorption material. The input data needed are the mass fraction of water in the air, the temperature on the surface of the sorbent and the area of each cell.
Analytical solution is obtained if the driving force of the adsorption process is a pressure gradient that means a pressure variation between vapour and the adsorbent surface. On that note, it is necessary to define the mass flux of water over the adsorbent surface as a function of pressure difference [37]. Considering the vapour as an ideal gas, the mass flux is:

$$\dot{m_{H2O}} = -D_{H2O} \cdot \frac{(p_v - p_{eq})}{RT} \qquad \left[\frac{kg}{m^2 s}\right]$$

Where:

- $D_{H2O}$ is the effective coefficient of water diffusion
- $p_v$ is the vapour partial pressure of the air mixture
- $p_{eq}$ is the vapour partial pressure in equilibrium condition between the adsorbent and the air mixture
- R is the ideal gas constant
- T is the temperature [K]

To take into account the mean size dimension of adsorbent pores and the mass of water molecules, the mass flux is multiplied by a global coefficient A:

$$\dot{m_{H2O}} = -D_{H2O} \cdot \frac{(p_v - p_{eq})}{RT} \cdot A \qquad \left[\frac{kg}{m^2 s}\right]$$

The partial pressures of vapour in the air mixture at initial conditions and at equilibrium condition are defined recalling thermodynamic relations describing vapour quality:

$$x = \frac{m_v}{m_{as}} \quad \left[\frac{kg_w}{kg_{as}}\right]$$

Where $m_v$ is the mass fraction of vapour and $m_{as}$ is the mass fraction of dry air. Considering the air as an ideal gas, the following expressions are valid:

$$m_v = \frac{p_v \cdot V}{R_v \cdot T}; \qquad [kg]$$

$$m_{as} = \frac{p_{as} \cdot V}{R_{as} \cdot T}; \qquad [kg]$$

The total mass of ambient air is equal to the sum of vapour and dry air mass fractions, so the pressure of the dry air can be consider as the difference of ambient pressure and vapour pressure. The ratio between gas constant of air and gas constant for water is equal to 0.662. Now, the vapour pressure is defined as:

$$p_v = \frac{x \cdot p_{amb}}{0.662 + x} \qquad [Pa]$$

At equilibrium condition the partial pressure of vapour is defined as:

$$p_{eq} = \frac{x_{eq} \cdot p_{amb}}{0.662 + x_{eq}} \qquad [Pa]$$

The vapour quality can be expressed as function of the igrometric grade of air, starting from its definition as ratio between partial vapour pressure and partial saturation pressure:

$$RH = \frac{p_v}{p_{v,sat}(T)}$$

So the expressions for initial condition and equilibrium condition are:

$$x = 0.662 \cdot \frac{RH \cdot p_{v,sat}}{p_{amb} - RH \cdot p_{v,sat}}$$

$$x_{eq} = 0.662 \cdot \frac{RH_{eq} \cdot p_{v,sat}}{p_{amb} - RH_{eq} \cdot p_{v,sat}}$$

where $p_{v,sat}$ is the saturation pressure which expression is found in literature [38]:

$$p_{v,sat} = 611.85 \cdot \exp\left(\frac{17.502 \cdot T}{240.9 + T}\right); \qquad [Pa]$$

$RH$ is the relative humidity at initial conditions, $RH_{eq}$ is the relative humidity at equilibrium conditions. $RH_{eq}$ depends on temperature of the adsorption material and on the bed humidity. The bed humidity can be interpreted as the moisture content inside the porous solid and therefore as the water quantity that the adsorbent material has gained during adsorption process. This is called water uptake W, and it can be calculated as [39]:

$$W = \frac{m(p_{h2o}, T_s) - m_0}{m_0} \qquad \left[\frac{kg_{H2O}}{kg_{dry\ bed}}\right]$$

Where $m(p_{h2o}, T_s)$ represent the weight of the material sample at given water vapour pressure and temperature of sorbate, and $m_0$ is the dry mass of the sorbate. Since the software calculates directly the material temperature for each cell on the surface of the adsorbent and the evaluation of W shall be made on each cell of the discretized domain, the idea at the base of implementation of water uptake into the CFD model is that one to define it as a new variable [40]:

$$W = W_0 + \frac{Total\ adsorbed\ mass}{\rho_s \cdot V_{cell}} \qquad \left[\frac{kg_{H2O}}{kg_{dry\ bed}}\right]$$

- $W_0$ is the water uptake at initial condition and its value depends on the cycle phase that we are considering: low value for adsorption, high value for desorption phase;
- $Total\ adsorbed\ mass$ is evaluated by the monitor tool of the software that sum the mass adsorbed during the whole transient of the process;
- $\rho_s$ is the solid density
- $V_{cell}$ is the volume of each cell.

For what concerns the volume of the cell, geometric consideration has to be done taking into account the symmetry of the system configuration, detailed in chapter 3.1.

The adsorption heat transfer is defined multiplying the water vaporization heat, assumed as hypothesis equal to 2500 kJ/kg, to the mass flux. The total heat flux on the surface of the adsorbent becomes:

$$\dot{Q}_{ads} = -\dot{m}_{H2o} \cdot H \qquad \left[\frac{W}{m^2}\right]$$

It should be noted that the mass flux and the heat flux have opposite working directions because the physic phenomenon of adsorption see the mass flux directed from air inlet towards the sorbent surface, and the heat generated is release outwards. The opposite happens for desorption process: the mass flux is directed outwards, while it is necessary to supply heat to drive the process. As consequence, the heat flux and mass flux should be defined with opposite sign.

## 3.1 Honeycomb configuration

As mentioned in the previous chapter 3, the volume cell equation depends on the geometry of the configuration of the system. The volume cell can be defined as follow:

$$V_{cell} = A_{cell} \cdot s \ [m^3]$$

Where $A_{cell}$ is the cell area, given by the software, and $s$ is the thickness of the cell that should simulate the thickness of the adsorption material. The honeycomb geometry is considered and it is shown in Figure 6:

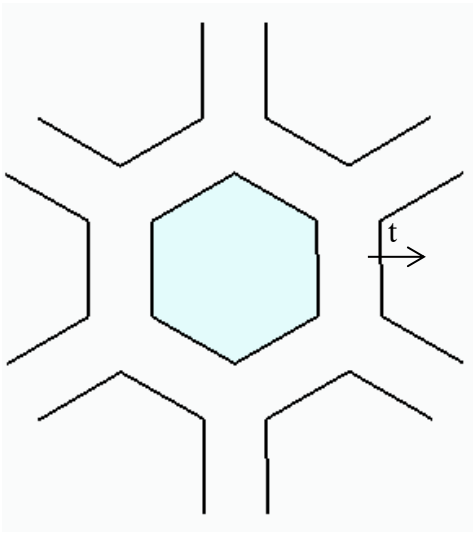


**Figure 6. Honeycomb geometry, frontal representation**

The alginate has a thickness equal to 2mm between air channels. Thanks to the symmetry of the configuration, it is easy to assume that the thickness of the cell is equal to half of the alginate thickness: $s = \frac{t}{2} = 1mm$.

The heat exchanger geometry is thought to maximize the efficiency of the adsorption process, which means that the system has to work with low pressure drop between inlet and outlet and high active surface area of adsorbent. But, as a matter of fact, high adsorbent surface area provokes also high pressure drop which means higher energy consumption for air recirculation. On the contrary low adsorbent surface area penalises water collection. As consequence, the maximum efficiency is obtained making a trade-off between the highest surface area that allows the lowest pressure drop.

Different geometry configurations of heat exchangers can be considered and in this case honeycomb-shape geometry is chosen.

Honeycomb configuration have been used widely in energy conversion technologies, such as gas separation by adsorption, compact heat exchanger, solar energy conversion and so on. In comparison with packed bed, honeycomb structures have the advantage to be characterized by a larger specific surface area that increases the efficacy of adsorption process and a significant reduction of pressure drop. From theoretical point of view, transport processes analysis in honeycomb configuration requires less empirical information. [41]

## 3.2 Determination of equilibrium relative humidity with alginate isotherms

To complete the adsorption model and apply mass flux and heat flux equations on the surface of the adsorbent, $RH_{eq}$ has to be evaluated as function of the porous solid temperature and the water uptake during transient. To do that, a family of adsorption isotherms characteristic for the alginate material is needed. Adsorption isotherms allows to evaluate the variation of the adsorbent capacity with respect to partial pressure of the adsorbate, maintaining a constant temperature. Each material, or adsorbent/adsorbate couple, is characterized by a specific type of isotherms. This addiction depends on material properties, such as its pore dimension and distribution, its tendency to bond with water and its coating capacity. Isotherm can be classified by IUPAC classification [42] in six principal families, shown in Figure 7:

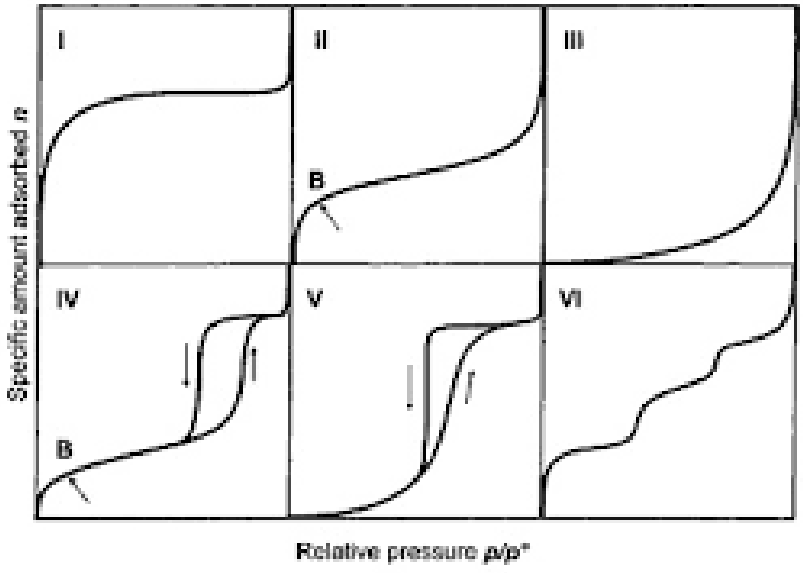


**Figure 7. IUPAC Isotherms classification [42]**

Considering the relative humidity is defined as the ratio between the vapour partial pressure and the saturation pressure, it is possible to evaluate the relative humidity in equilibrium conditions by means of alginate isotherms. Usually, the experimental construction of the isotherm curves is conducted at different temperature and partial pressure conditions, weighting material samples during an adsorption process to evaluate the specific amount adsorbed inside. In case of alginate with 10% of $CaCl_2$, isotherms between 20°C and 60°C, with an interval of 10°C, are studied. The following graph shows the water uptake in relation to the relative humidity for 20°C, 40°C and 60°C temperature case with each regression line.

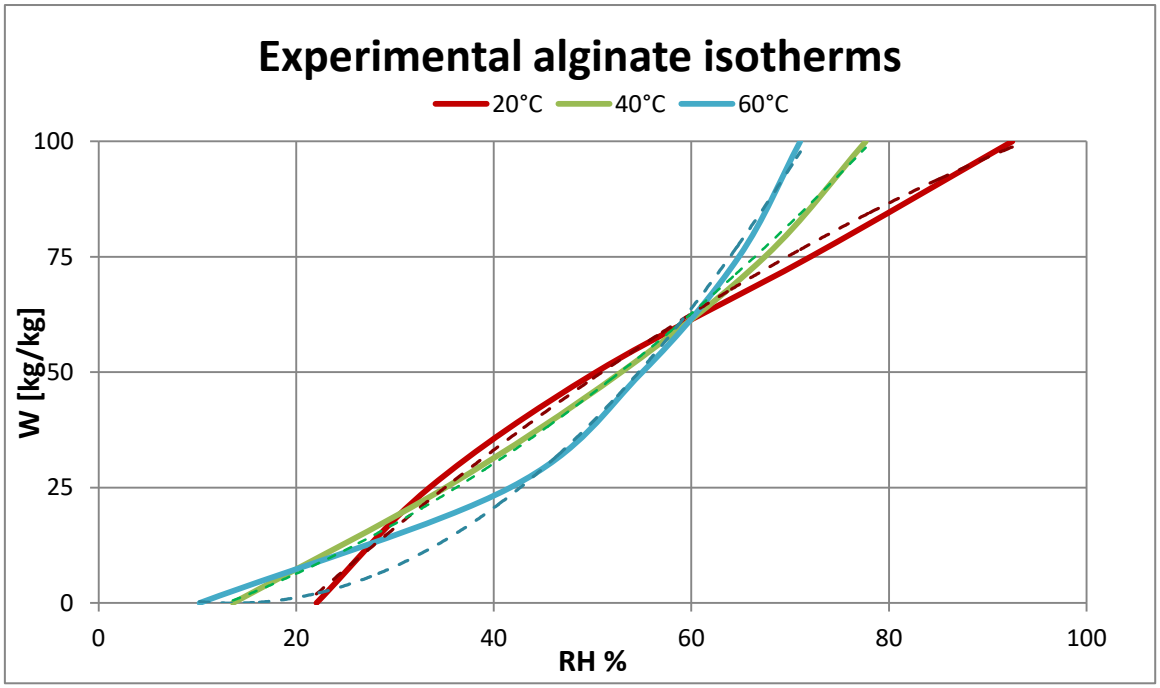


**Graph 1Experimental Alginate Isotherms for temperature of 20°C 40°C 60°C**

The implementation of $RH_{eq}$ depends hence on sorbent temperature T and its water uptake W, so after the estimation of experimental isotherms, a polynomial regression is calculated for temperature of 20°C, 40°C, 60°C. The regression is made thanks to MATLAB function, able to correlate multidimensional data in polynomial equation [43]. As result, a third order polynomial is obtained:

$$RH_{eq} = a0 + a1 \cdot T + a2 \cdot T^2 + a3 \cdot W + a4 \cdot W \cdot T + a5 \cdot W \cdot T^2 + a6 \cdot W^2 + a7 \cdot W^2 \cdot T + a8 \cdot W^3 + a9 \cdot T^3$$

Where the experimental coefficients $a_n$ are resumed in table:

| | |
|---|---|
| **a0** | 0 |
| **a1** | 1.054E-02 |
| **a2** | -1.9023E-04 |
| **a3** | 7.5014E-01 |
| **a4** | 2.0333E-03 |
| **a5** | -3.9615E-05 |
| **a6** | -1.7062E-01 |
| **a7** | 1.1364E-03 |
| **a8** | 1.3276E-05 |
| **a9** | 8.5969E-07 |

**Table 3 Experimental coefficient of third grade regression equation**

The MATLAB MultiPolyRegression of $RH_{eq}$ is plotted in figure 9:

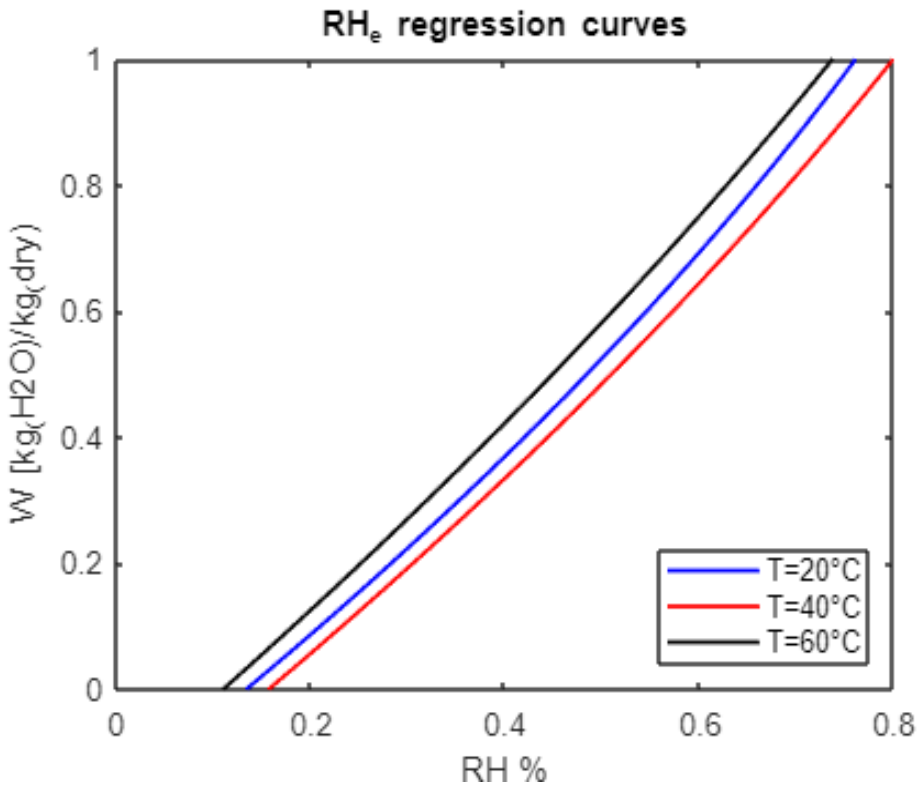


**Figure 8. Regression curve of $RH_{eq}$ for 20, 40, 60°C**

A way to compare the goodness of the regression is that one to calculate the relative error between experimental data of W and the resulting from the regression. Table 3.1 resumes all data collected:

| RH [%] | Temperature [°C] | W test [kg/kg] | W regression [kg/kg] | Relative error [%] |
|---|---|---|---|---|
| 22.05254 | 20 | 0 | 1.96 | / |
| 33.48996 | 20 | 25 | 22.39 | 10.44 |
| 50.34045 | 20 | 50 | 49.20 | 1.60 |
| 72.04998 | 20 | 75 | 77.96 | 3.94 |
| 92.48783 | 20 | 100 | 99.1 | 0.9 |
| 13.59654 | 40 | 0 | 0.54 | / |
| 35.10992 | 40 | 25 | 23.54 | 5.84 |
| 52.88981 | 40 | 50 | 50.10 | 0.2 |
| 67.43307 | 40 | 75 | 76.89 | 2.52 |
| 77.65535 | 40 | 100 | 98.46 | 1.54 |
| 10.21985 | 60 | 0 | 0.31 | / |
| 41.66454 | 60 | 25 | 23.37 | 6.52 |
| 55.02911 | 60 | 50 | 50.96 | 1.92 |
| 64.80881 | 60 | 75 | 77.87 | 3.82 |
| 71.02268 | 60 | 100 | 97.93 | 2.07 |

**Table 4 Comparison between W tested and W regression**

Looking the relative error, we can notice that at low relative humidity, indeed lower water uptake, the regression values do not fit the experimental data. In fact, for W= 0.25 (kg/kg), the relative error reaches a maximum of 10%. On the contrary, at higher RH > 50%, the relative error decrease in the order of 2-3%. This deviation from experimental data affects the simulation, in particular during regeneration phase of the process, when RH is lower than adsorption phase.

The implementation of $RH_{eq}$ in STAR-CCM+ requires an additional adjustment: since the regression depends on temperature, negative oscillations are expected at high temperature, like >60°C. So a maximum constraint is applied in the way that $RH_{eq}$ function assumes the value 0 instead of negative values.

# Chapter 4

# Alginate adiabatic adsorption simulations

The adsorption heat exchanger (HEX) is made by alginate-based adsorbent, organized in honeycomb structure column among which fins are placed. The system is simulated by the software STAR-CCM+, through a CFD analysis in order to evaluate the water uptake of the sorbent and its response to the dynamic of adsorption/desorption process. In particular, in the present chapter two configurations are studied. The first one represents a single air volume with hexagonal shape, on whose surface area the model is applied. The case of adiabatic adsorption is investigated, highlighting the main properties of alginate-based adsorbent.

The second configuration represents the finned heat exchanger: a single air volume is presented coupled with solid adsorbent, on which the variation of temperature is studied. The model is modified to simulate a coated configuration where heat flux and temperature profile are investigated on the interface between air region and solid region, divided by a thin void layer that represent the coating.

To perform an adequate simulation several steps have to be respected. First of all the geometry of the system is developed according to the dimension of the component studied. The HEX device is 10x12 cm of area and has a 2.5 cm of length. A portion of the adsorbent area is shown in figure:

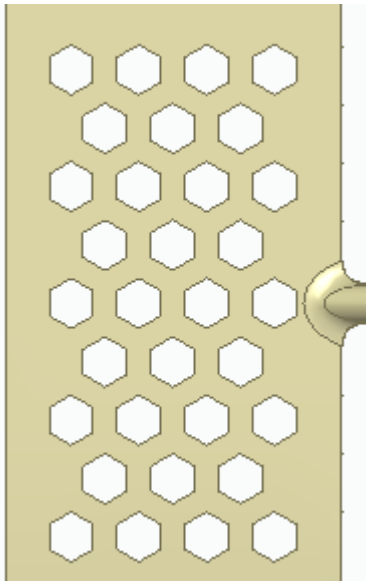

**Figure 9. Frontal view of the alginate-based heat exchanger**

To reduce the computational cost, a single adsorption unit is simulated. A unit is considered to be an air channel. For this reason the starter geometry has the dimension of an hexagonal volume of side equal to 2.6 mm and length of 25 mm. The geometry figured represents the air volume contained in a channel of the adsorption heat exchanger.

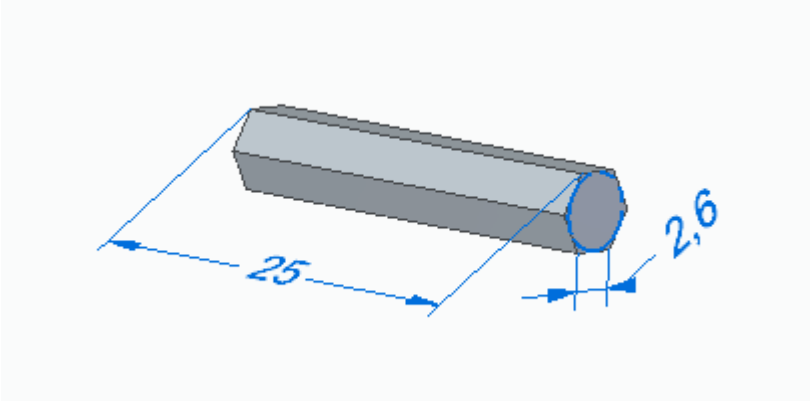


**Figure 10. Air volume of HEX channel**

After the creation of geometry part, the domain is discretized by *Automated mesh* tool of the software. A volume mesh is created choosing the criteria:

- Surface Remesher
- Automatic Surface Repair
- Polyhedral Mesher
- Prism Layer Mesher

The mesh is built setting a base size equal to *5E-04 m* to guarantee a good accuracy of the results. Prism layers are set up equal to 4, with the Prism Layer Stretching function equal to 1.3 that progressively increases the height of the prism layer of 30% with respect to the previous layer. The built mesh is shown in the following figure:

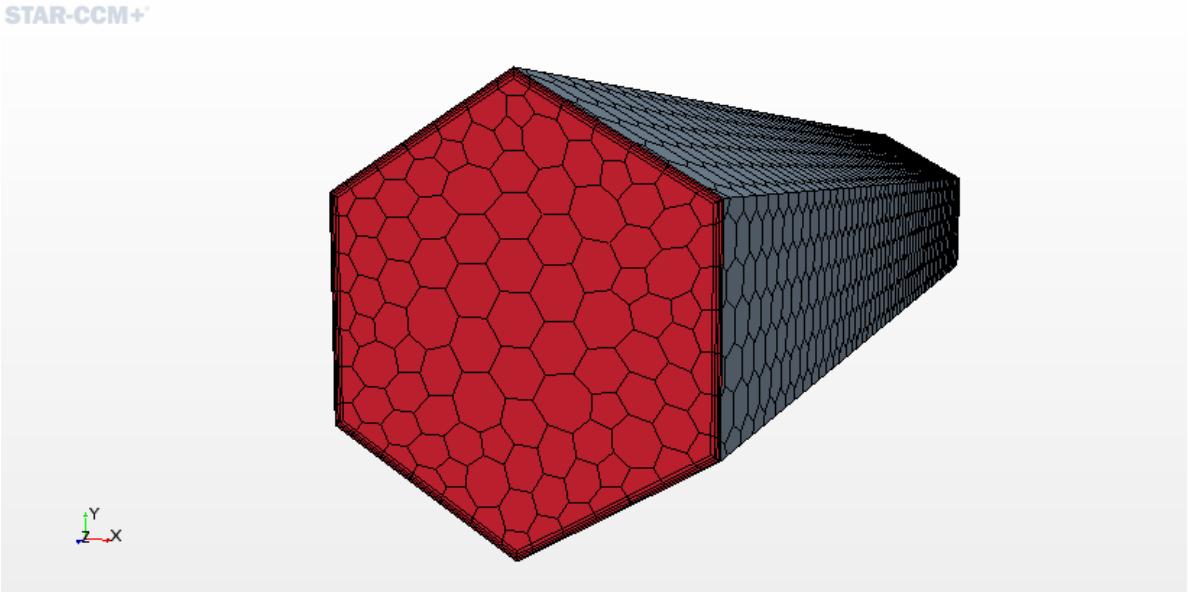


**Figure 11. Mesh view of air volume**

After the definition of the geometry and its discretization by volume mesh, the physics of the model is set up. In this case only air contained in the heat exchanger is simulated. It is necessary define a single physics continuum that considers the air as a mixture gas with water vapour. The software proposes default models to build specific physics continuum. In this case the chosen models are listed below:

- Three Dimensional
- Implicit Unsteady
- Multi-Component Gas
- Ideal Gas
- Non reacting
- Segregated flow
- Segregated Fluid Temperature
- Segregated Species
- Laminar

Implicit unsteady model has the function to control the update at each physical time for the calculation and the time-step size in which chosen Inner Iterations are solved. Multi-Component Gas model is used to implement air and water properties as a gas mixture. In addition, Non-Reacting model say that the components of gas mixture do no interact. Ideal Gas model is chosen to calculate the density of the medium as a function of temperature and pressure. Segregated Flow, Segregated Fluid Temperature and Segregated Species solve respectively momentum, energy and continuity equations: the enthalpy is computed starting from the temperature. In conclusion the process is supposed to be laminar, because of low velocity field applied to the system.

The next step sees the implementation of the theoretical equations describing adsorption phenomena using *User-defined Field Functions*. All the field functions are defined as scalar and are used to implement equations mention in chapter 3 and all that constants needed to characterize the system and the materials involved. A summary of the constants and of the variables used are reported in tables 5 and 6:

| Name | Definition |
|---|---|
| Initial water uptake | 0.0026 [$kg_{H2O}/kg_{dry}$] |
| Alginate density | 700 [$kg/m^3$] |
| Water diffusion coefficient | 4E-07 |

**Table 5. Constants model parametres**

| Name |
|---|
| Adsorbed mass specific |
| Heat flux |
| Mass flux |
| X_moisture |
| Pv_H2O |
| x_eq |
| Pv_eq |
| Pv_Saturation |
| RH_air |
| RH_eq |
| W |

**Table 6. List of Field functions of adsorption model**

Each defined function is solved for all the cells and for each iteration. Moreover, the water uptake, set as a input variable, depends on the *Field Sum Monitor*, whose function is that one to sum up the mass adsorbed for each time-step. In that case, the mass adsorbed is considered per unit of adsorbent mass.

Once defined the physics continuum, boundary conditions are imposed. In particular, air inlet and outlet conditions are set on the forward and backward areas of the channel, assigning the initial conditions of the process and hexagonal lateral surface is that one where adsorption model is defined.

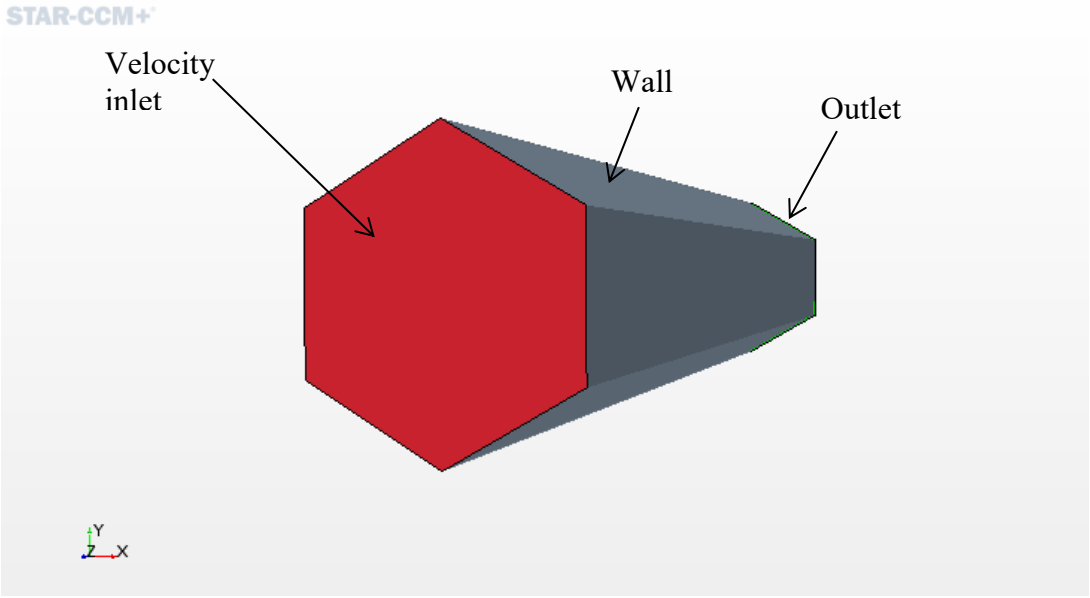


**Figure 12. Boundary conditions of air volume**

As shown in figure 15, at inlet boundary a *Velocity Inlet* condition is applied imposing the following initial conditions:

| | |
|---|---|
| Mass fraction | 0.011 of water, 0.989 of air |
| Temperature [°C] | 25 |
| Velocity [m/s] | 0.3 |

**Table 7. Initial conditions**

At outlet, a condition named *Outlet* is imposed. The action of this condition is to define the split ratio of flow, namely how much flow exits the boundary. It is set equal to 1 to say no flow split.

On the hexagonal surface a *Wall* condition is imposed: *Thermal Specification* is set to Heat Flux and the field function that evaluates the Adsorption Heat Flux is assigned; *Wall species Option* is set to Specified Flux and the Method is chosen in the way to define different condition for each component of the mixture. From the moment that the idea is that one to study the amount of water collected on the surface of the domain, air component is set to 0 [kg/m$^2$s], water component is assigned to the field function defined to evaluated the Mass Flux of water. Both heat flux and mass flux are calculated for each cell.

The total model is now set and can run. Before starting the simulation, a series of pre-processing conditions are imposed. As the problem is Implicit Unsteady, each physical time-step involves a number of Inner iteration to converge the solution for that given instant of time. However, setting the right number of inner iteration per time step is not trivial: generally inner iteration number is determine observing its effects on the result. Small physical time means the solution is changing less from one time step to another, and so less inner iteration is required, and vice versa. In this case a time-step of 30s and a number of inner iteration equal to 100 are chosen as a good balance between transient accuracy and computational cost.

When the solver is run, a discretized version of model equations are solved for each cell in the mesh: the residual in each cell represents the degree to which the discretized equation is satisfied [44] and it represent the absolute error of a particular variable studied. A perfectly converged solution is characterized by residual equal to machine precision. A plot of residual for this simulation is reported in figure 16:

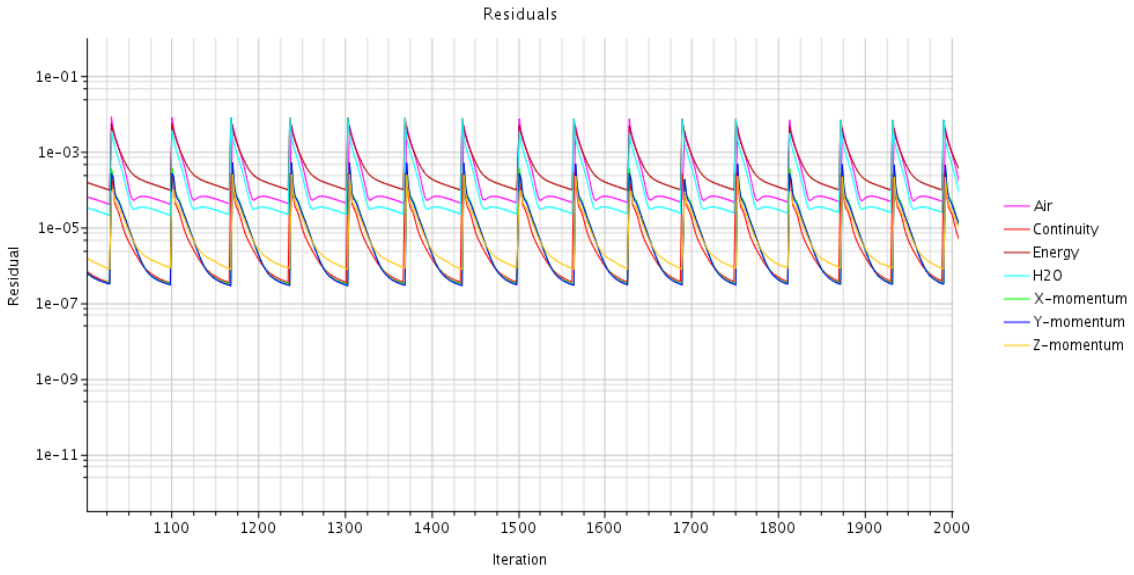


**Figure 13. Residual plot**

We can see that the stopping criteria defined per each inner iteration are solved in the time step chosen. Stopping criteria are satisfied when reach a value of 1E-04. The maximum physical time is set to permit the simulation to converge and stop it when the transient is complete. A value of 22000s was imposed to the adsorption phase, equal to that one of experimental isotherm tests.

## 4.1 Adiabatic simulation results

Simulation results are shown in this chapter. The post-processing creates a series of plots and scenes from report tool, in order to monitored the convergence of the simulation, the dynamic evolution of variables during transient and so the variable values at convergence. The results obtained from adiabatic adsorption process are reported in graphs below. Particular attention is given to the amount of water mass adsorbed, indeed the water uptake of the adsorbent material, the moisture content and the temperature between inlet and outlet. The simulation computes an adsorption cycle at initial conditions of temperature equal to 25°C and relative humidity of the air equal to 60%.

The water uptake is shown in figure 17. The value reached at convergence is equal to 0.65, that means a water gain of 65% with respect to the dry material.

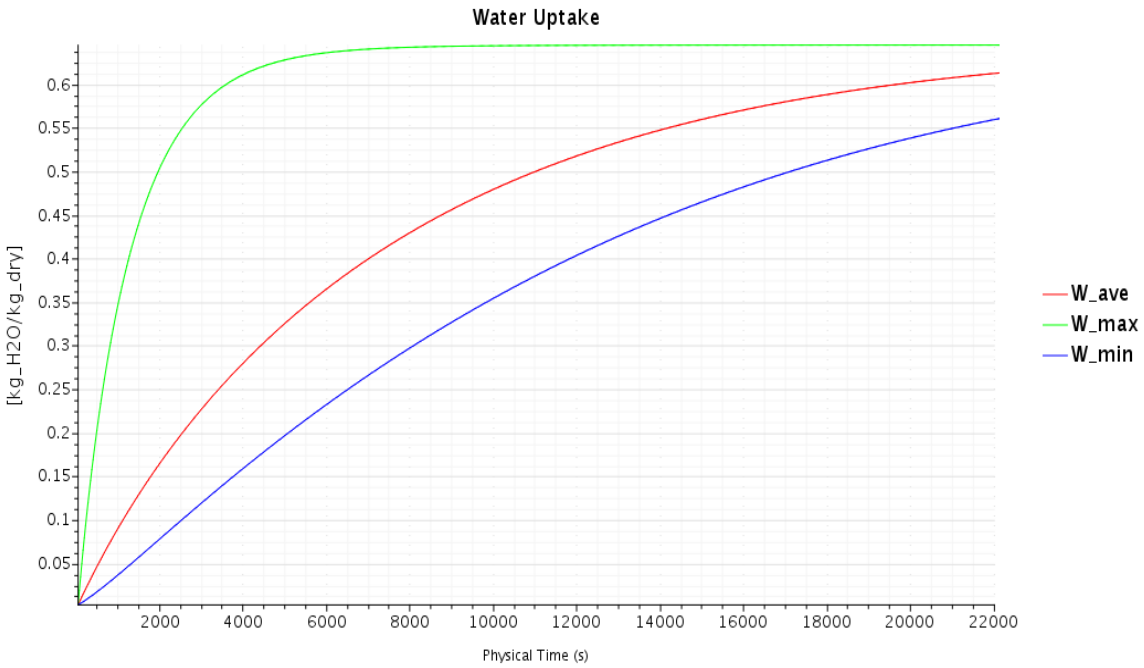


**Figure 14. Water Uptake during adsorption process**

A series of scenes concerning the water uptake is reported for different simulation times. The time evolution is controlled by the time steps of 5, 100, 250 and 500. One time-step is 30s of physical time.

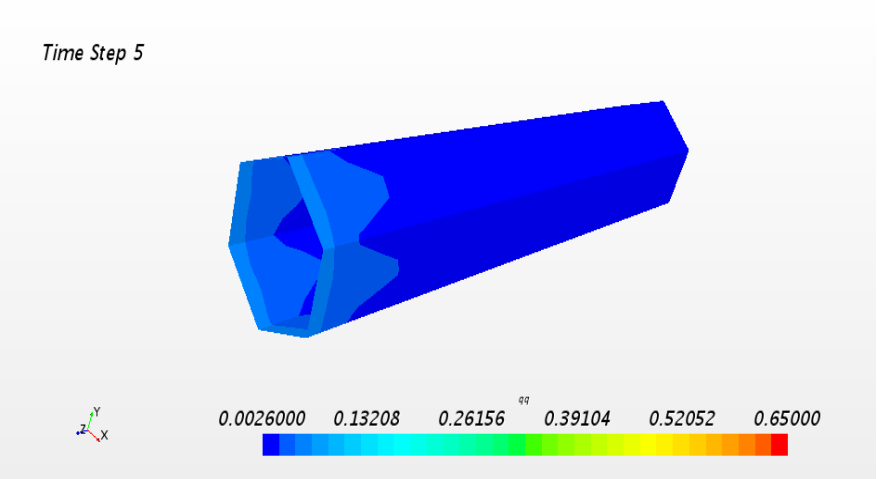


**Figure 15. Water uptake at Time-step 5**

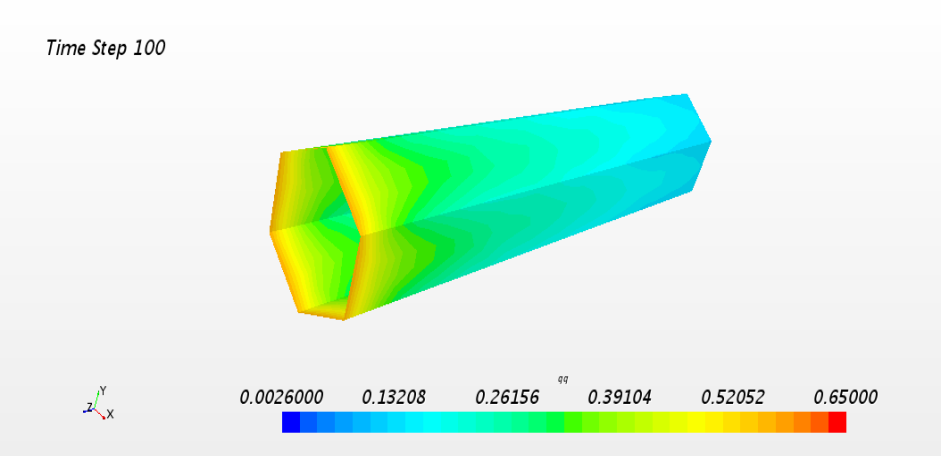


**Figure 16. Water uptake at Time-step 100**

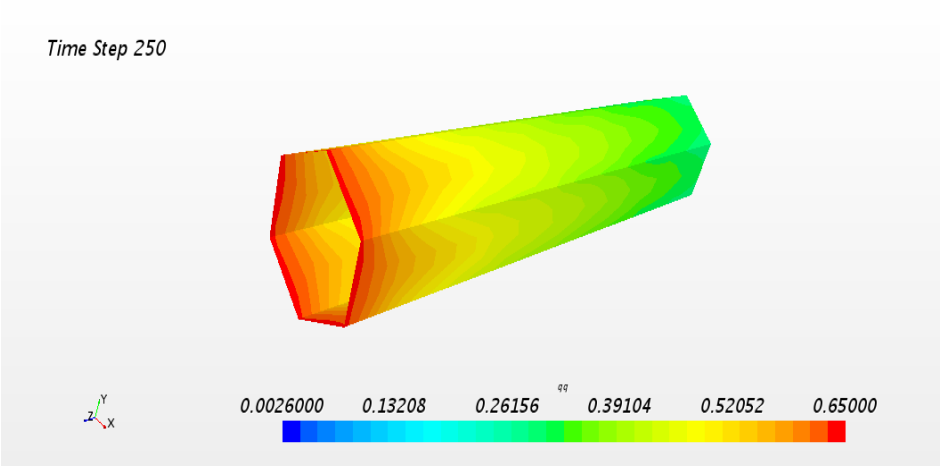


**Figure 17. Water uptake at Time-step 250**

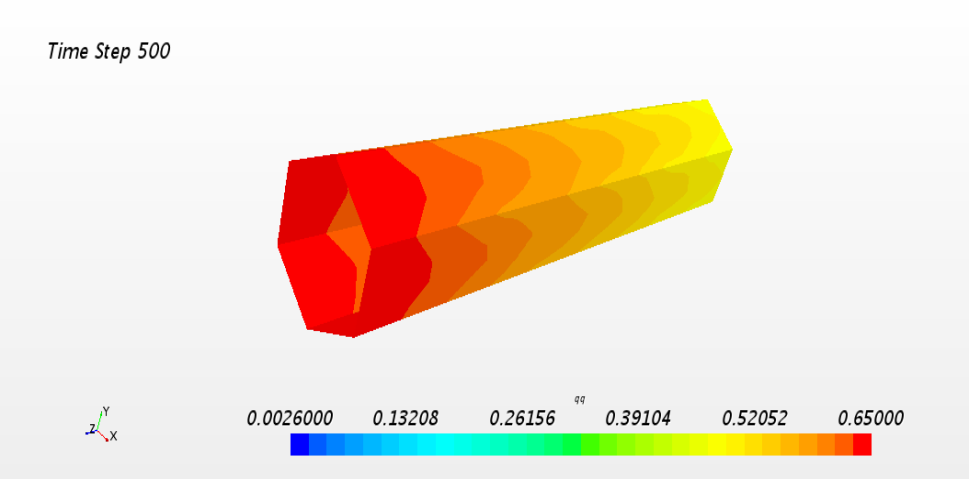


**Figure 18. Water uptake at Time-step 500**

The scenes show the variation of water uptake on the surface of the volume domain. As the model is applied on the external area of an air volume, other regions do not present variation of W. At the beginning of the simulation, the material is supposed to be dry. To express that situation an initial condition of water uptake is set to be equal to 0.0026 $kg_{H2O}/kg_{dry}$. At the end of the simulation the total surface area is at the maximum value of water uptake, that depends on the initial conditions of inlet air temperature and relative humidity, imposed equal to 25°C and 60% respectively. These values are respected in comparison with that one experienced in experimental isotherm curves tests.

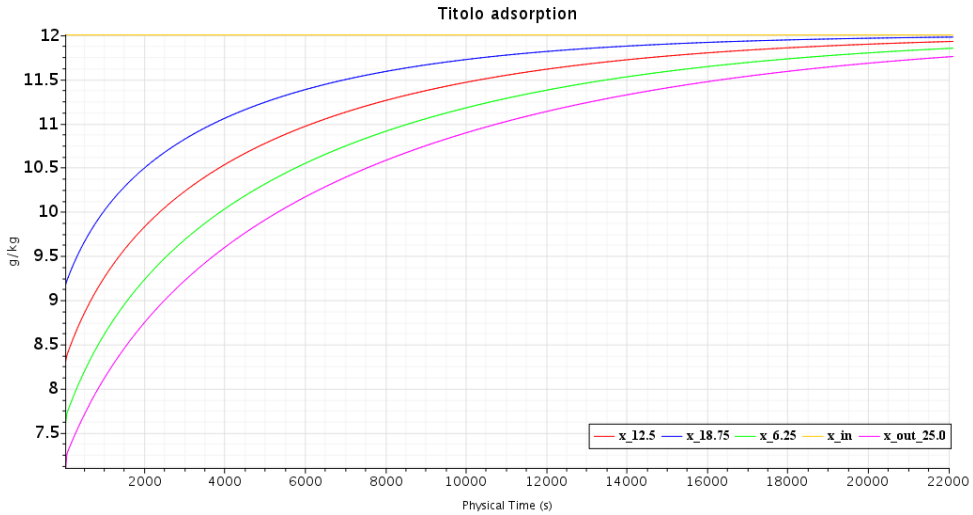


**Figure 19. Water concentration during adiabatic adsorption**

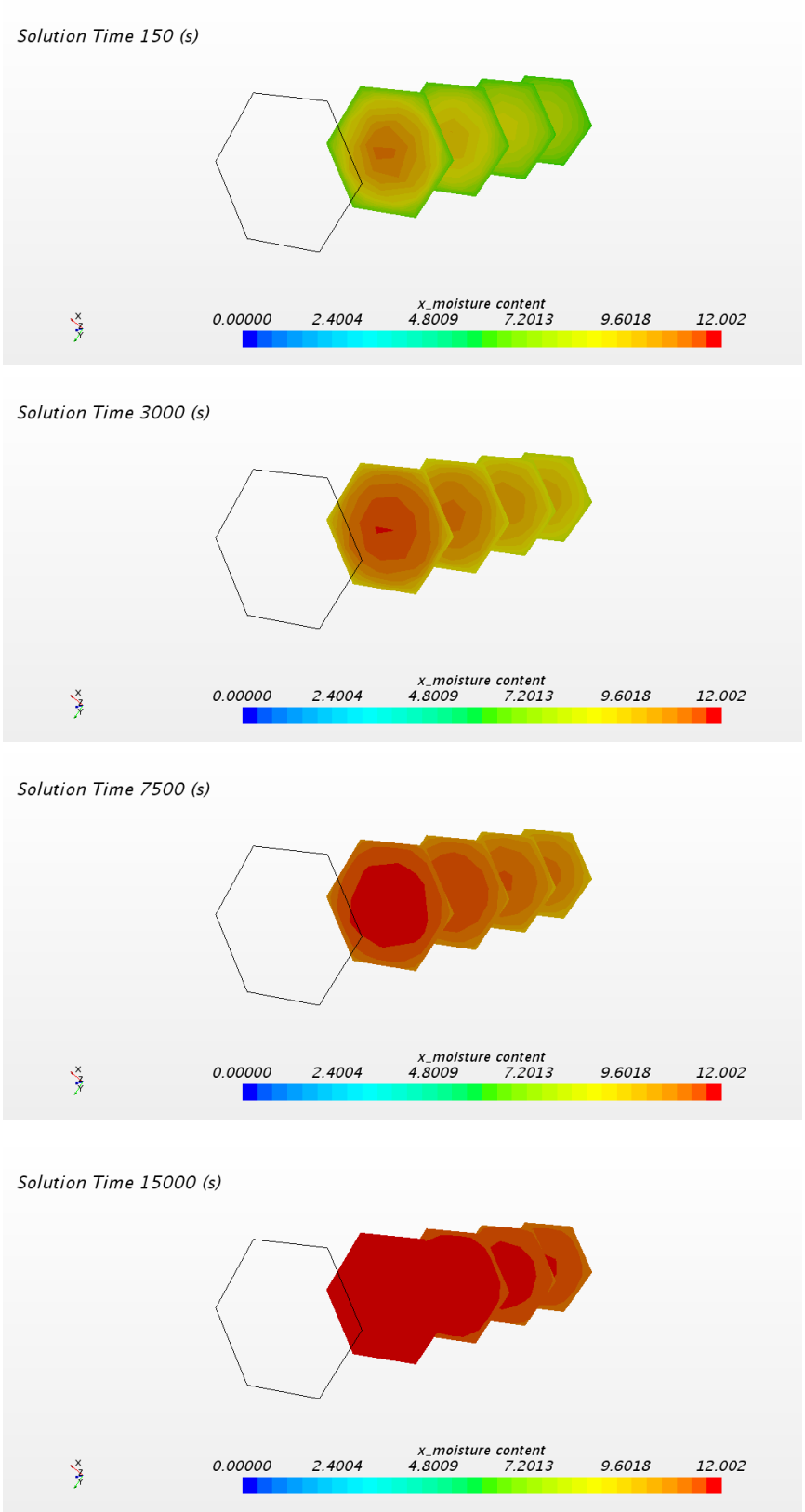


**Figure 20. Water concentration during adiabatic adsorption for 150, 3000, 7500 15000s**

Similar comments are done for the water concentration: the variation in time of the quantity studied is reported in three main scenes, at 150s, 3000s, 7500 and 15000s. The scenes show five sections which include the whole length of the geometry. The inlet face is shown only as a reference because it represents the inlet velocity condition, that means it correspond to the maximum water concentration achievable. Other sections are located at 6.25mm, 12.50mm, 18.75mm and 25.00mm. As expected, the concentration of water increases with time and reaches convergence value equal to the inlet condition at the end of the transient. Each section achieves the convergence in different time moments that increases with the distance from inlet face. This behaviour is due to the fact the material reaches saturation gradually in space, and obviously in time, and the results confirm it.

Another plot of interest is the pressure drop between inlet and outlet boundary. This report calculate the difference of pressure between two different boundaries or interfaces. As mention in chapter 3, adsorption process is driven by a pressure driving force between initial condition and equilibrium condition. At the beginning of the simulation the pressure drop is relatively high and at the end, as the material achieves equilibrium, tends to 0.

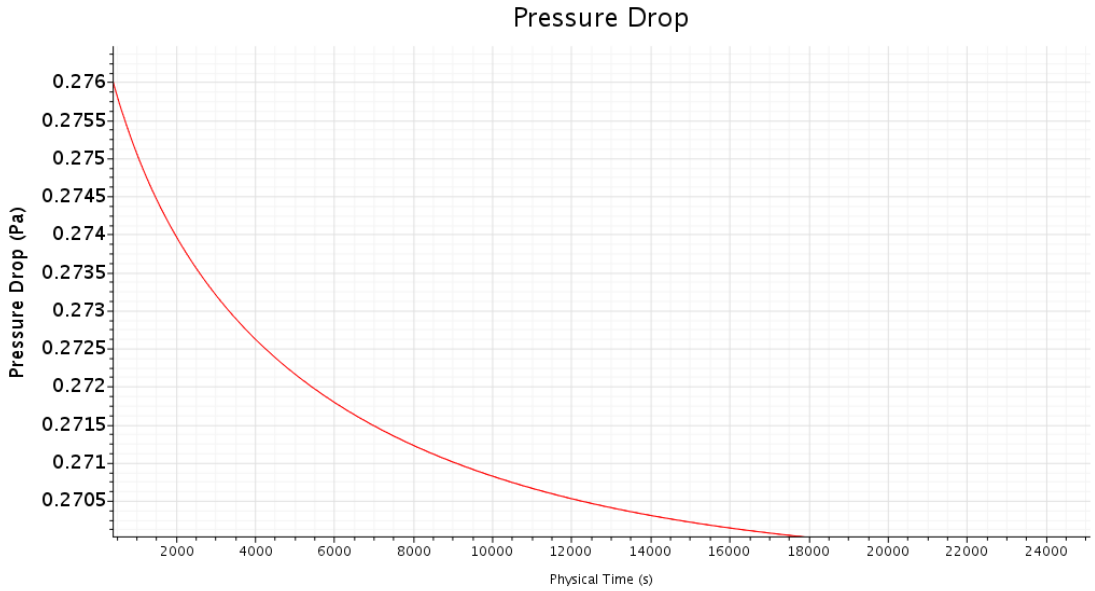


**Figure 21. Pressure trend during adiabatic adsorption**

## 4.2 Independent grid study

One of the principal aspect that affects CFD simulations is the quality of the their meshes. For this reason the following chapter treats about the meaning of mesh in qualitative terms and address the study towards a sensitivity analysis of grid independence. The results of a numerical simulation is strongly dependent on its mesh that influences also the computational time of the simulation. The balance between a good mesh and a reasonable solution time is not trivial. Independence grid study is based on the idea to prove the quality of the solution demonstrating a chosen quantity is independent from the refinement of the mesh, that means mesh size does not affected the convergence and the values of the solution.

### 4.2.1 Volume Mesh Theory

A mesh is a discretized representation of a geometric domain. This domain include geometry and its content. For this discussion the Finite Volume Method (FV) is used as discretization method. It is a numerical technique, able to transforms "*partial differential equations representing conservation laws over differential volumes into discrete algebraic equations over finite volumes*" [45].

The integral form of the conservation equation used as starting point is defined assuming the velocity field and the fluid properties are known. The general form of conservation equation for the quantity $\Phi$ is [46]:

$$\int_S^l \rho\Phi\mathbf{v}\cdot\mathbf{n}\,dS = \int_S^l \Gamma\,\nabla\Phi\cdot\mathbf{n}\,dS + \int_V^l q_\Phi\,dV$$

Where the first member represent the diffusion transport in which $\Gamma$ is the diffusivity of $\Phi$, and the second member is the source term in which $q_\Phi$ is the source of $\Phi$.

The distribution of $\Phi$ has to be discretized, so the domain is divided into finite numbers of small control volumes creating a grid which defines their boundaries. Any type of grid can be accommodated and related to a coordinate system. The conservation equation is applied at the centre of each cells in the way that surfaces integrals are the same for that control volumes which share boundary. The discrete values of $\Phi$ are computed by solving a set of

algebraic equation deriving from the conservation equation. This process is called discretization process.

In general the FV approach is chosen because it is the simplest in comparison with the Finite Difference Method, but it requires three levels of approximation which are interpolation, differentiation and integration[47]. Furthermore there are some properties that allow to say Finite Volume Method is favourable with respect to other method:

- Conservation equation terms are turned into face fluxes and evaluated at faces of finite volumes. This method is strictly conservative because of the flux entering a volume is the same of that one outgoing the adjacent volume.
- It can be formulated in the physical space on unstructured polygonal meshes.
- Since the unknown variables are evaluated at the centroids of the volume elements, it is quite easy to implement different type of boundary conditions in a non-invasive manner.

### 4.2.2 Step of discretization process

The generation of the mesh sees the replacement of continuous domain by a discrete one: the first step of the solution process is the discretization of the geometry in non-overlapping elements delimitated by a set of faces and the definition of physical boundaries by the marking of the boundary faces.

Then, algebraic equations are obtained by integrating over each discrete element the partial differential equations. The system of algebraic equations is solved in order to compute dependent variable values for each element.

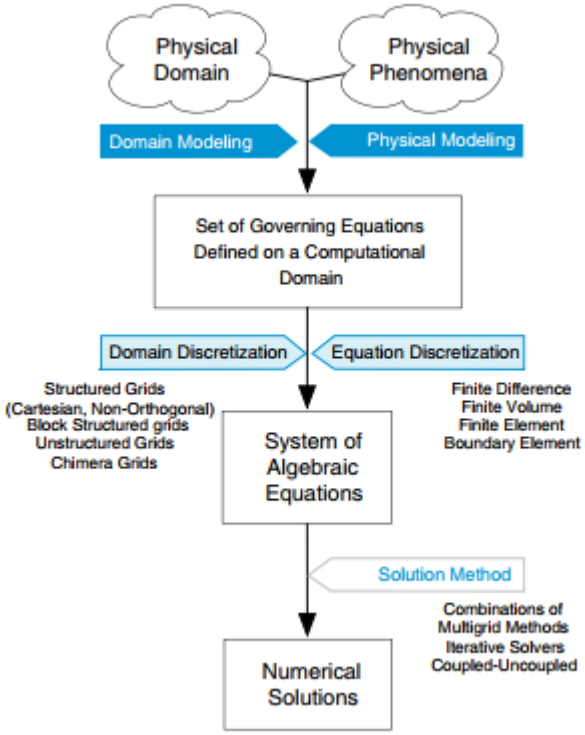


**Figure 22. Step of discretization process**

The method is complete capturing the topological information about discrete elements arrangement and their relations.

### 4.2.3 STAR-CCM+ mesh implementation

Simcenter STAR-CCM+ solvers find solutions to physics equations at the locations defined by the mesh. Volume mesh can be generated automatically or they can be user-guided.

In this case, an automatic mesh is chosen. It typically contains irregular mesh structures and is generated using tetrahedral, hexahedral, or polyhedral cells. Refinements can be carried out where needed.

Once design the geometry the next step is to build the mesh . The following models are chosen:

- Surface Remesher
- Polyhedral Mesher
- Prism layer Mesher

Typically, the initial surface of a geometry is made up of triangulated surfaces, also called tessellation, where the triangles are highly skewed and not suitable for generating a high-quality volume mesh. For this reason, Surface Remesher is needed in order to improve the overall quality of the mesh, remeshing the initial surface of the geometry generating more evenly-size triangles.

The polyhedral meshing model uses an arbitrary polyhedral cell shape in order to build the core mesh [44], in particular a special dualization scheme is used to create the polyhedral mesh from an underlying tetrahedral mesh. The polyhedral cells created typically have an average of 14 cell faces.

In comparison with tetrahedral meshing, polyhedral meshing has some advantages that can be resumes as follow: thanks to the many neighbours gradients and local flow distributions are better approximated; even if more neighbouring cells means more storage and computing operations per cell, the final solution has higher accuracy(4); polyhedral cells are less sensitive to stretching; smart grid generation and optimization techniques offer a high number of possibilities because cells can automatically be joined, split, or modified by introducing additional points, edges and faces.

Prism layer mesher is used to generate orthogonal prismatic cells next to wall surfaces or boundaries and it is necessary to have higher accuracy of the solution. Prism layers also allow high aspect ratio cells, reduces numerical diffusion near the wall because aligns flow with the mesh.

After choice the mesher models, the automatic mesh is created. A series of default control are set in order to obtain a volume cell distribution able to guarantee a likely solution. One of the default control that most influences the mesh is the base size, that determine the length of each cell base.

The sensitivity analysis is performed changing the base size of the mesh and run the simulation in order to compare the results of a particular variable. Water up take “W” is chosen as variable.

### 4.2.4 Results

Simulation is run changing the mesh refinement, in particular the base size values are reported in table 8, while the other default controls are kept unchanged.

| Base Size [mm] |
|---|
| **0.5** |
| **0.75** |
| **1** |
| **2** |
| **3** |

**Table 8. Mesh base size**

Water up take is showed in the following graph for different base sizes. The solution time during which the quantity is evaluated, is 60 minutes:

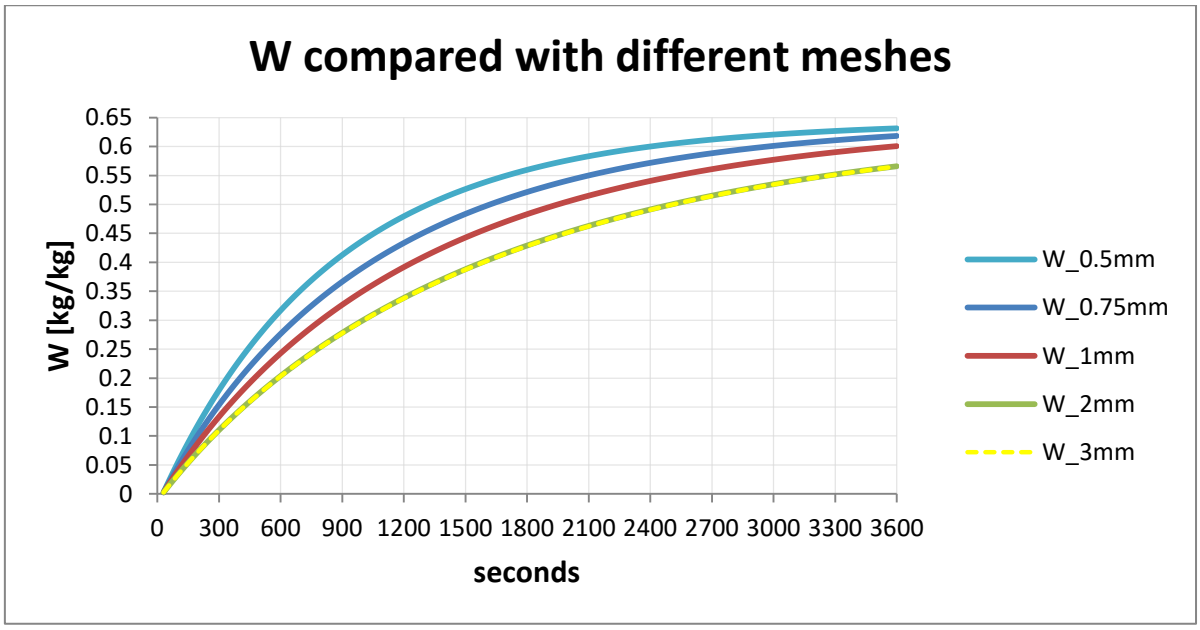


**Graph 2. Comparison with different meshes base size**

All trends differs from the 0.5mm curve, but the most different trends are observed for 2 mm and 3 mm base size meshes that coincide. To balance a good approximation with a relatively low computational cost, the coarsest mesh which is not affected too much by the refinement of the mesh is chosen to be 0.75 mm base size mesh. After 60 minutes, the 0.5mm and 0.75mm curves seems to converge, while the other curves not.

Time solution is compared for each base size case. The graph shows solver elapsed time per time step that is how long the software takes to execute the last time step. This solver is typical of unsteady simulation.

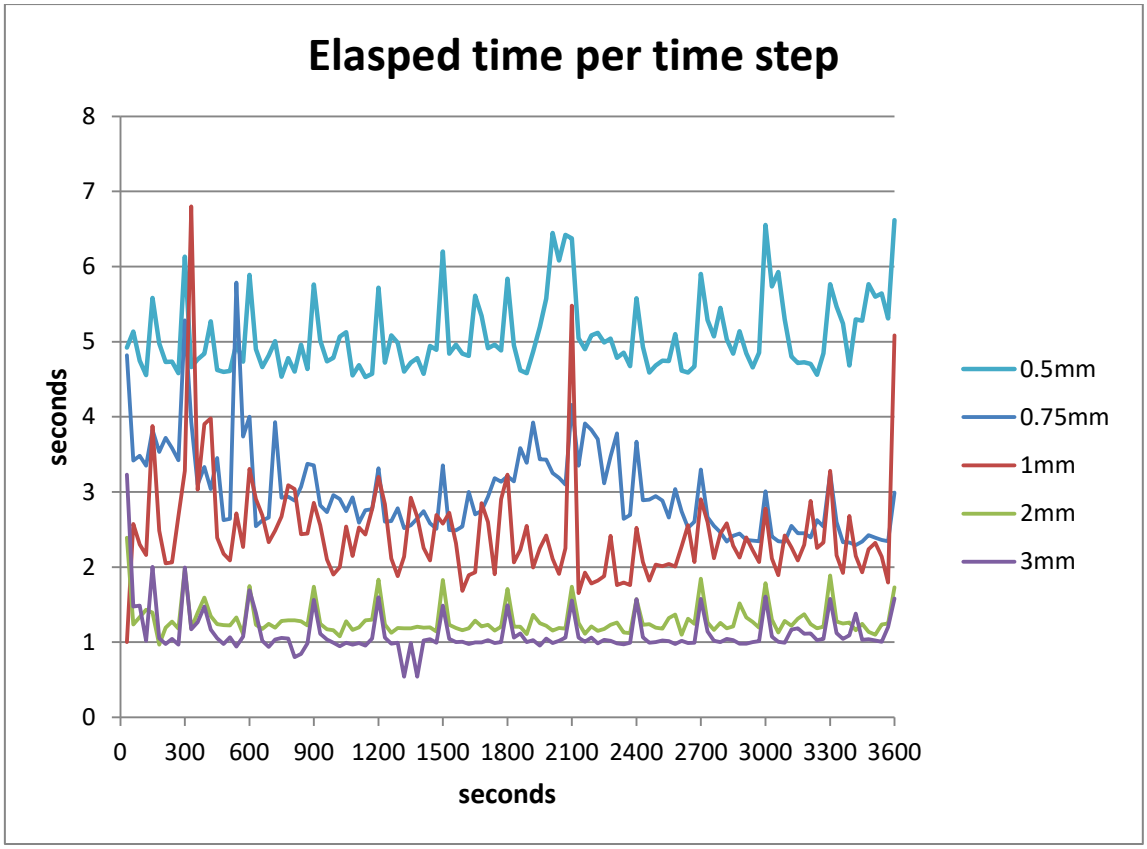


**Graph 3 Elapsed time per time step of different base size meshes**

In addition it is possible to compare the total solver elapsed time, that represents the cumulative time taken to run the entire solution. After 60 minutes the total elapsed time is shown in graph 4:

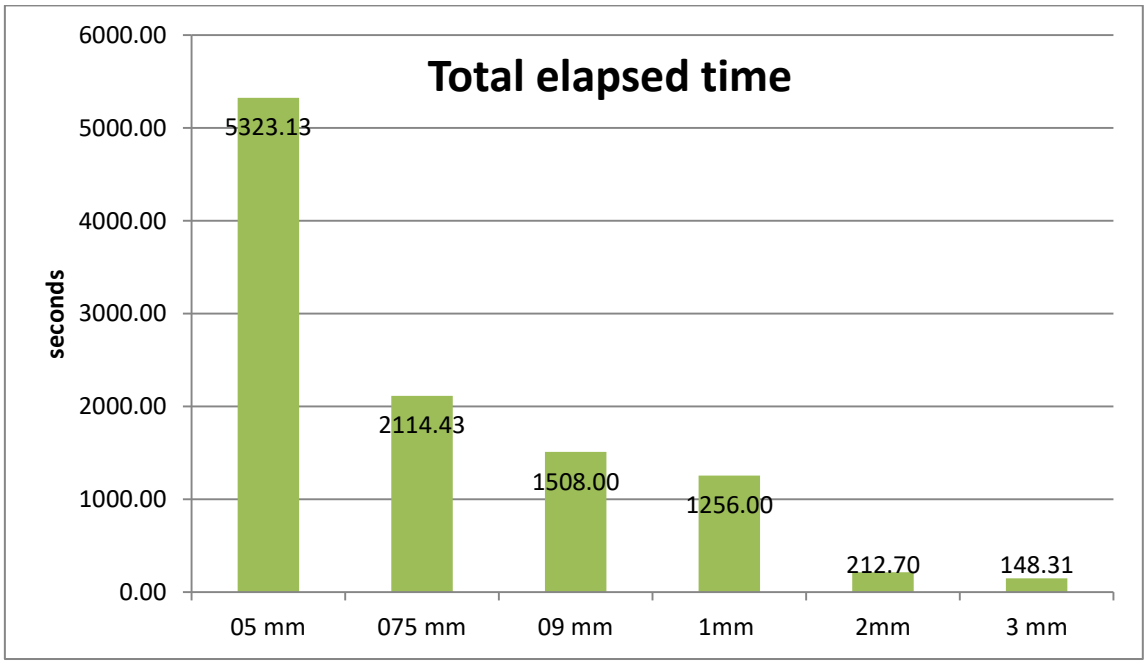


**Graph 4. Total elapsed time**

As seen in the histogram, the time needed to run the 3 mm base size simulation is about 33 times lower than the 0.5 mm base size simulation. It is obvious that this aspect impacts on the choice of mesh size.

As results of the analysis, the 0.75mm base size mesh is the coarse one that does not affected the final result of the water uptake value. The computational cost in term of time is lower than almost 3 times the 0.5mm one.

In conclusion, STAR CCM+ offers several tools to check mesh quality, like mesh Diagnostics tool, used as reference (not a guarantee of a converged solution) . The report given by Diagnostic tool summarizes the entity count, mesh extents and mesh quality. By means of Threshold values, identification and visualization of cell can be performed. This tool allows to check skewness angle, face validity, cell quality and volume change. As a guide line, following values are suggested for mesh quality metric by the *User guide line* of STAR CCM+:

| | Suggested values |
|---|---|
| Minimum face validity | 0.95 to 0.51 |
| Minimum cell quality | 1e-05 to 1e-12 |
| Minimum volume change | 1e-05 to 1e-12 |
| Minimum contiguous cells | 1 to 1.000.000 |

**Table 9**

Poor quality cells created during the mesh generation process can be identified and removed by using the Remove Invalid Cells tool. This tool is targeted at removing disconnected cells, or near zero volume cells. The solver can handle the cells with marginal cell quality.

# Chapter 5

# Coating adsorption model

The configuration studied in this work is a finned heat exchanger that performs adsorption with alginate-based material. The model that describes the process is simulated in the adiabatic case, without taking into account the presence of porous adsorbent and the presence of the fins, that particularly influence the regeneration process. The idea is to complete the model in order to compare the simulated solution with experimental data resulting from the test on the alginate-based heat exchanger. The test is conducted in order to evaluate the temperature gradient of the alginate during transient heating phase of regeneration process. Hence, a solid part has to be added to the model to represent the adsorbent. This kind of operation meets some impossibilities related to the software logics. First of all, thinking to couple a fluid region in contact with a solid region is the trivial way to consider the adsorption coating, specifically the surface in contact where the water mass flux is simulated. But the software does not allow to impose a mass flux on a boundary referring to a solid. So, the adsorption model cannot be solved on the surface in between air volume and solid volume because of solid constraint. In addition, to drive regeneration a fin temperature profile has to be set on the solid region and has to influence the air region, that means heat flux and temperature are imposed on the same boundary and it is not allowed too.

The solution is found coupling the coating region and the air region with a thin void in between. They do not have interface and as consequences the adsorption model can be applied. The water mass flux condition is applied on the air volume surface and also the temperature profile of the fin. At the same moment the temperature profile of the fin is calculated on the solid region considering the effects of recirculating water temperature, set as input, and the adsorption heat generation.

To make this feature consistent with respect the reality of the phenomenon, in addition to the initial hypothesis of neglecting diffusion of vapour through adsorbent pores and of considering the adsorption heat generated as a constant, a new hypothesis is set:

- The thermal resistance of the coating is neglected.

This is possible because, considering the thermal conductivity of the adsorbent and the thickness of the coating, enough low thermal resistance is obtained. Numerically, the thickness of the coating is usually less than *1mm* and the thermal conductivity of an adsorbent is in the range of *0.4-0.2 W/mK*. So the resistance is of the order of $10^{-3}$.

As result, the temperature on the interface between the fin and the coating is equal to the temperature on the interface between coating and air.

The implementation of this extension to the adiabatic adsorption model is done by means of Data Mappers tool of the software STAR-CCM+.

The geometry is built accordingly to that one expose in the previous chapter 3.1. The whole domain studied has the dimension of an hexagon of side equal to 2,6mm and length of 25mm inscribed in a rectangular block of the same length. The distance between air volume and solid volume is imposed to be $t_c = 0.5\ mm$ and is set as the thickness in the definition of the volume cell. This parameter influences the evaluation of the water uptake since its definition is:

$$W = \frac{Total\ adsorbed\ mass}{\rho_s \cdot V_{cell}}$$

and the volume is $V_{cell} = A_{cell} \cdot t_c$

The system geometry is presented in figure 26:

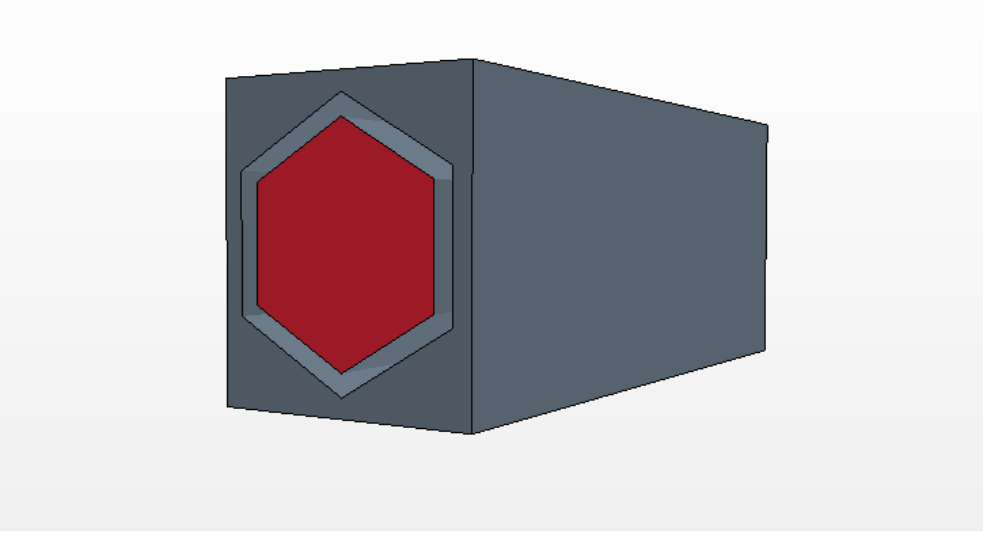

**Figure 23. Geometry domain of Coated HEX unit**

All the simulations are carried out considering half of the domain, thanks to the symmetry of the geometry. In this way the computational cost is halved.
Following the simulation construction routine, after the definition of the geometry parts, the mesh is built, each for different regions. Both meshes are generated by the following models:

- Surface Remesher
- Automatic Surface Repair
- Polyhedral Mesher
- Prism Layer Mesher

For air region a base size of 5E-04 m is chosen and for the adsorbent a base size of 1E-03. Coupling different meshes can cause problem with the model solution, so a *Surface control mesh* is applied to the faces related in order to apply to them the same base size of 5E-04.

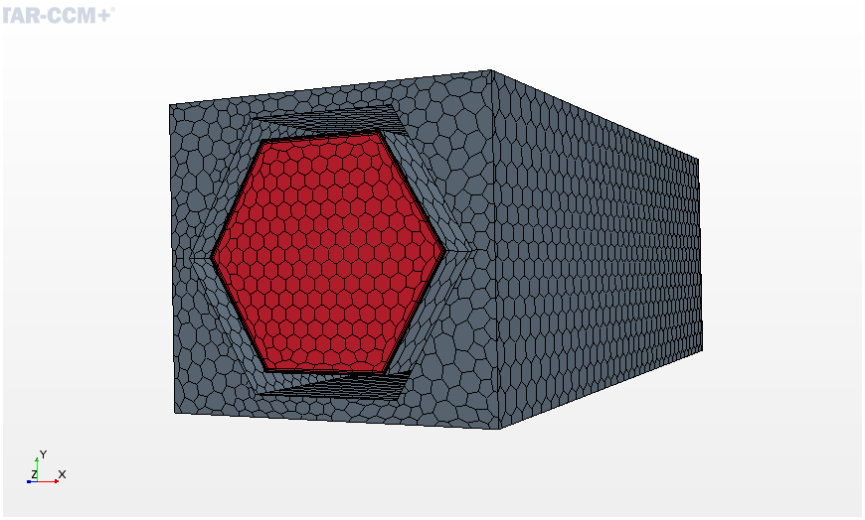

**Figure 24. mesh of Coated HEX unit**

Two physics continua are then created: one for air region and one for solid region. In the same way of adiabatic adsorption simulations, the air physics continuum is made by the following models:

- Three Dimensional
- Implicit Unsteady
- Multi-component Gas

- Non-reacting
- Ideal gas
- Segregated Flow
- Gradients
- Segregated Fluid Temperature
- Segregated Species
- Laminar

A new physic continuum to describe the adsorption material is set as follow:

- Three Dimensional
- Implicit Unsteady
- Solid
- Constant density
- Segregated Solid Energy
- Gradients

The Solid model give the possibility to choose different materials from software database. Since the alginate is not present, its properties are set manually. In particular the thermal capacity is set equal to Silica Gel one because there no reference in literature. The properties used are in table 10:

| Name | Definition |
|---|---|
| Thermal capacity | 1000 kJ/kgK |
| Alginate density | 700 [kg/m$^3$] |
| Thermal conductivity | 0.21 W/mK |

**Table 10. Alginate properties**

As in the previous chapter, the *User-defined Field Functions* are used to describe the adsorption process. The next step sees the definition of the boundary conditions. With respect to the adiabatic model, the heat flux evaluated on the hexagonal surface of the air volume, now has to be assign on the adsorbent face. At the same way the temperature profile

of the adsorbent material has to be assigned to the hexagonal surface of the air region. To do that, *Data Mappers* tool is used. A Data Mapper allows to interpolate field data on a surface mesh or a volume mesh so that the mapped fields can be used for applying boundary or volume conditions on the target mesh [48]

Two surface to surface Data mappers are set for heat flux and temperature:

- Heat Flux: the Field Function set to obtain the Adsorption heat flux is associated to this map in order to use it to define the boundary condition of the internal surface of the adsorbent.
- Temperature of the solid: maps the temperature profile at the internal surface of the solid and it is used to define the boundary condition of the hexagonal surface in the air volume.

The other boundary conditions are set subsequently, depending on the region. In air region, *at inlet boundary a* Velocity Inlet condition is applied imposing the following initial conditions:

| | |
|---|---|
| **Mass fraction** | 0.011 of water, 0.989 of air |
| **Temperature [°C]** | 25 |
| **Velocity [m/s]** | 0.2 |

**Table 11. Initial condition of velocity inlet boundary**

At outlet the flow split outlet is set. Different with respect to the adiabatic boundary setting, at hexagonal surface *Thermal Specification* is set to Temperature and the method chooses the field function *"Mapped Temperature*", created when the *Data Mapper* is set, while *Wall Species* remains set in the way to calculate the mass flux for water component of the mixture.

In solid region, Left and Right boundary are set as *Wall*, with *Thermal Specification* fixed at constant temperature that depends on the phase of the process. For instance, during adsorption a temperature of 20°C is chosen, while during regeneration a temperature of 60°C is preferred.

The inlet and outlet boundaries are set as adiabatic Wall, and for the other opposite two walls a Periodic Interface is created. The last but not least boundary to set is that one

internal: *Thermal Specification* is Heat Flux, and by the field function method the "Mapped Adsorption Heat Flux" is chosen from the list.

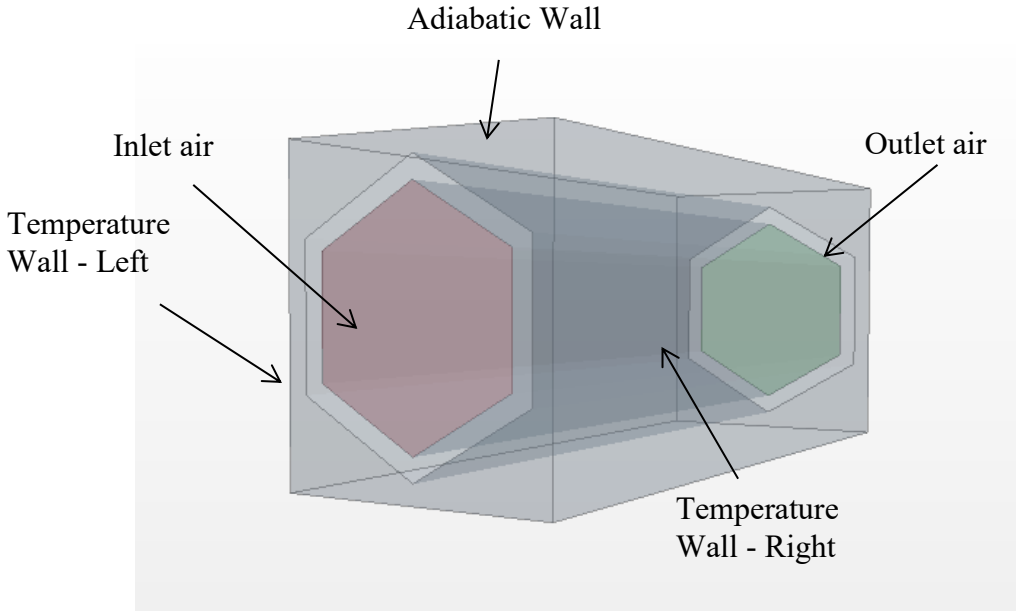


**Figure 25. Boundary conditions**

.

As final step for setting the simulation, solvers has to be imposed. A time-step of 30s and Inner Iterations equal to 25 are chosen. The simulation computes for 6000s for adsorption phase and 3000s for regeneration phase.

Finally, the post-processing collects several data in plots and scenes. In particular the adsorption/desorption cycle is shown. The initial conditions for each phase are resumed in table 12:

| | Adsorption | Desorption |
|---|---|---|
| Time | 60 min | 60 min |
| Velocity | 0.2 m/s | 0.2 m/s |
| RH | 60% | 60% |
| T adsorbent | 21°C | 60°C |
| T air | 25°C | 25°C |

**Table 12. Initial condition of the whole transient**

The water uptake achieved on the adsorbent surface is reported with the relative humidity variation in air for both adsorption and desorption cycles and with the air temperature.

The water uptake reach the 100% of gain in mass. That means that the alginate dry weight is insignificant in comparison with the water weight adsorbent. This validate the properties of alginate described in chapter 2.

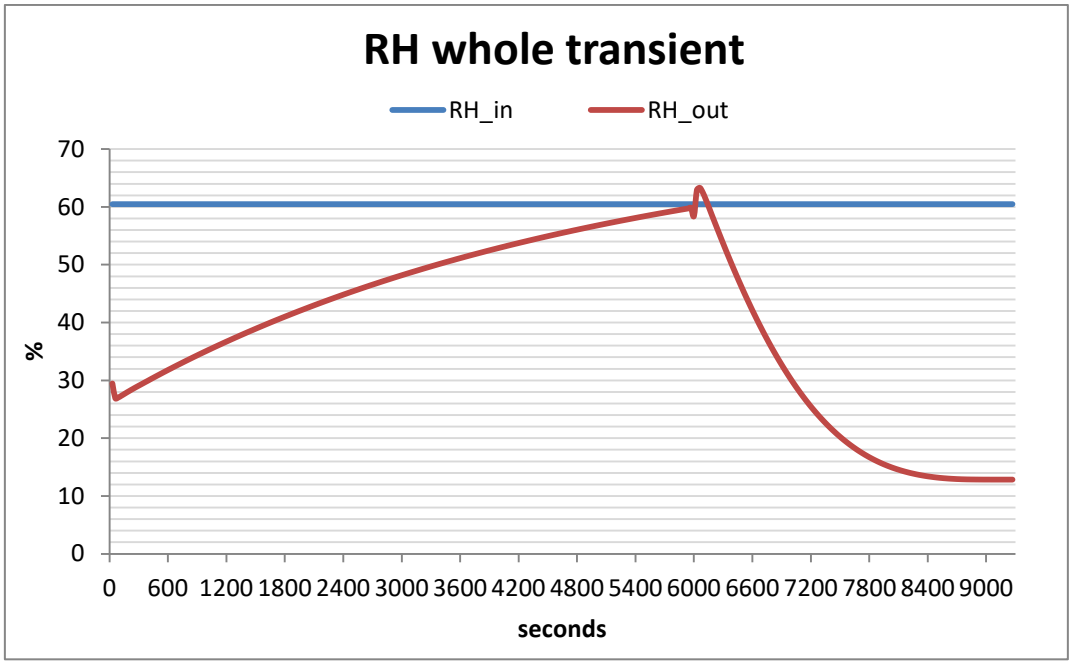


**Graph 5. RH whole transient of Coated HEX unit**

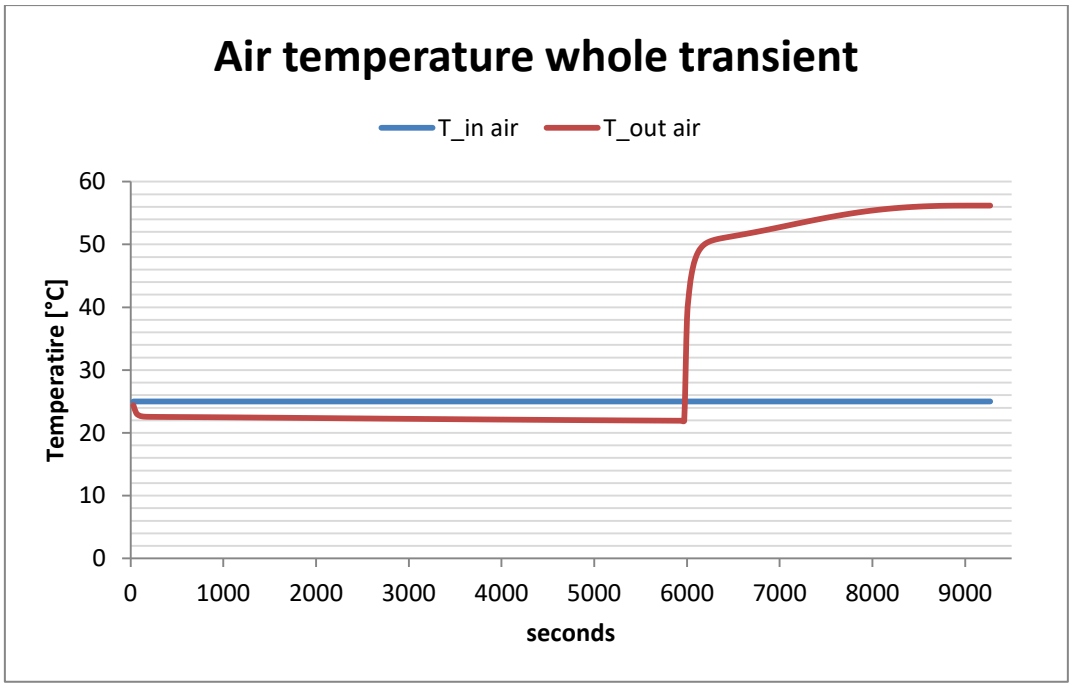


**Graph 6. Air temperature whole transient of Coated HEX unit**

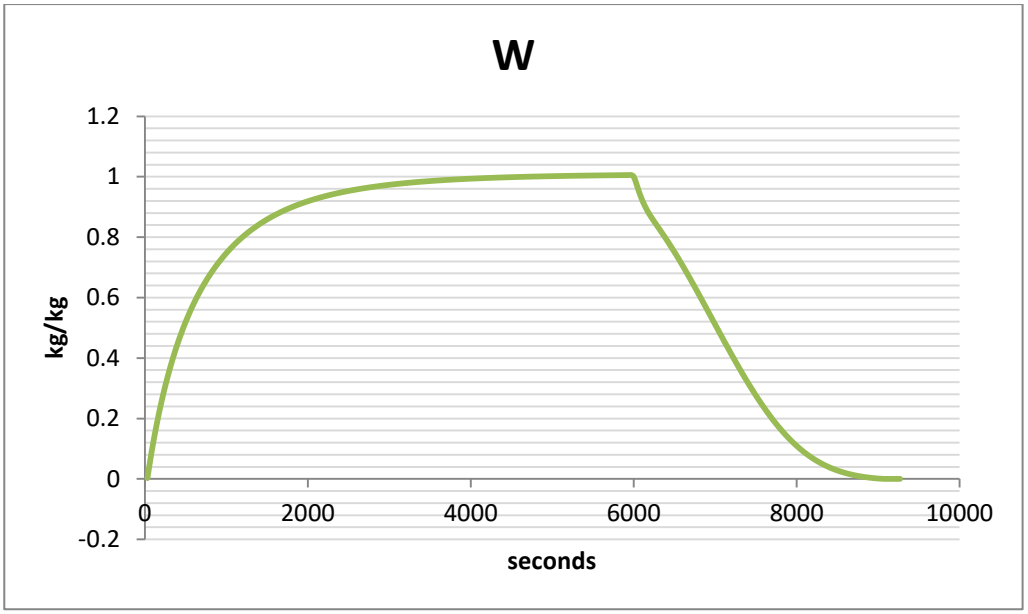


**Graph 7. Water uptake of the whole transient of Coated HEX unit**

## 5.1 Experimental evaluation of temperature gradient in alginate-based heat exchanger

The material considered is characterized by analysing its behaviour during a transient in order to evaluate its properties. The goal of this chapter is to gauge the temperature variation in time of the alginate, heated up by a water recirculation system. The experiment is carried out by the use of a thermal imaging camera, that capture the infrared radiation of the heating material and gives the temperature of the heated device in each point.

### 5.1.1 Initial conditions

The temperature measurements are done starting from ambient condition. The objet under study is considered has the same properties of a grey body. Initial condition are resumed in the following table:

| | |
|---|---|
| Temperature | 15°C |
| Emissivity | 0.9 |
| Reflection temperature | 25°C |

**Table 13**

The ambient temperature is that one of DENERG Laboratory of Politecnico di Torino ambient condition in winter season.

The emissivity, that describes the capacity of a body to emit electromagnetic radiations and is specific for each material, depends on the temperature, the wave length of the radiation and the superficial finishing of the object in question. For engineering study the emissivity of a grey body is considered wave length independent on its surface, and roughness independent. In particular, metals have low emissivity and non-metal materials have an high emissivity grade, that in this latter case permits to measure easily superficial temperature with infrared camera. For these considerations and these initial temperature conditions, an average emissivity of 0.9 is chosen to describe the organic material. The reflectivity of the body is evaluated introducing a corrective factor, which in this case is the reflected temperature. In the most situation this temperature corresponds to ambient temperature and in the case of high emissivity field the effects of this correction are very low.

A sensitivity analysis is carried out to demonstrate the reflection temperature does not influence the temperature field. Considering different values of temperature, the reflection temperature is modified to see how much affect the values considered:

| Reference temperature [°C] | Test [°C] | Reflection temperature [°C] |
|---|---|---|
| 20 | 20.6 | 20.00 |
| | 20.0 | 25.00 |
| | 19.9 | 26.00 |
| | 19.4 | 30.00 |
| 44 | 44.4 | 20.00 |
| | 44.0 | 25.00 |
| | 43.9 | 26.00 |
| | 43.5 | 30.00 |
| 83 | 83.3 | 20.00 |
| | 83.0 | 25.00 |
| | 82.9 | 26.00 |
| | 82.6 | 30.00 |

**Table 14. Reflection temperature analysis**

A variation of 10°C of the reflection temperature corresponds to a variation of 1.2°C in case of 20°C, 0.9°C in case of 44°C, and 0.7°C in case of 83°C.

It is likely that reflection temperature does not influence the measurements, so it is considered equal the default thermo-camera setting.

### 5.1.2 Characteristic of the thermal imager

The experiment is carried out using a TESTO 875i, thermal imaging camera suitable for thermography applications. Superficial temperature is capture by the camera thanks to infrared sensor, able to convert thermal energy into an electronic signal, then elaborated it into images. The no contact measurements are displayed and saved by the camera. It is possible to post-process each image by the software IRSoft.

The thermo-camera works in a range of temperature between -30°C and 550°C, adaptable to experiment requirements and has a thermal sensitivity < 50 mK at +30 °C. In particular, there are three types of measuring field with different precision:

| Measuring range | Temperature range | Accuracy |
|---|---|---|
| Measuring range 1 | -30°C to +100°C | ±2°C<br>(±3 °C of m.v. at -30 to -22 °C) |
| Measuring range 2 | 0°C to +350°C | ±2 °C |
| High temperature measuring | +350 to +550°C | ±3 °C |

**Table 15. Accuracy of thermo imager**

Other characteristics are described in table 16.

| **Focus** | **manual** |
|---|---|
| **Infrared resolution** | 160 x 120 pixels |
| **Image refresh rate** | 33 Hz |
| **SuperResolution (Pixel)** | 320 x 240 pixels |
| **Minimum focus distance** | 0.1 m (Tele: 0.5 m) |
| **Field of view** | 32° x 23° |
| **Thermal sensitivity** | < 50 mK at +30 °C |

**Table 16. Characteristics of thermo-camera**

The functions and the accuracy of this type of instrument are suitable for the experiment.

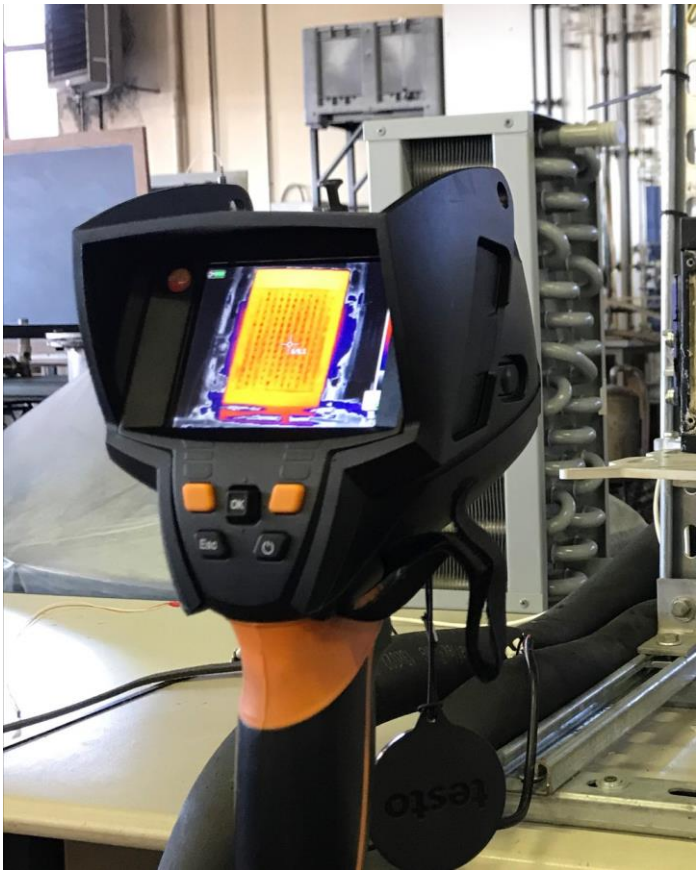


**Figure 26. Thermo-imager 875i**

### 5.1.3 Experiment set up and procedure

The system is composed of an heat exchanger coupled with alginate plate, obtained by 3D printing technique. The alginate plate has hexagonal holes where air is free to flow. It is arranged in a grid 10x12cm, in the way that aluminium fins are interpose between two hexagonal hole columns. The heat exchanger device works thanks to the application of a resistance and a pump, connected with tubes to a water tank characterized by a capacity of 30L. The tubes are equipped with valves that allow to regulate the flow of water from the tank to the adsorber device. Resistance and pump  heat and circulate hot water through the device respectively, to promote the heat transfer and so the adsorption/desorption process.
The system heating process is studied by the use of the infrared thermo-imager. The camera is set up to Measuring Temperature Range 1, between -30°C and 100°C and the measuring function is 1 point type. Infrared images are taken from a distance of 50cm and with a variable time step. The maximum temperature and the thermal capacity of the adsorber are

unknown, so the time step chosen is small enough to evaluate the temperature gradient with sufficient accuracy.

**Procedure**

The thermo-imager is set before starting the test. The test procedure can be described in some passages:

1. the tank is filled by tap water in the way to cover the resistance positioned inside. Then the resistance inside the tank is switched on. To isolate the heat exchanger from the heat sink, two valves are incorporated on the inlet and outlet tubes. At the beginning the valves are closed. In this way the water is heated up inside the tank for about 1.5h
2. The thermo-imager is positioned in front of the heat exchanger on top of an easel, in the way to frame the part of device containing the alginate, at distance of about 50 cm. A first image of ambient condition, at time 0, is taken.
3. When the water is near to the boiling point, the valves are opened and the pump is activate for water recirculating through the device.
4. While the system is heating up, the thermo-camera takes picture each 10s for the first 4 minutes and each 30s for the next 21 minutes. The infrared pictures are taken manually because the camera has not a timer function or video function.
5. At the end of the testing time (25 minutes) the resistance and the pump are switch off and the tank cools down naturally.

The test take place in DENERG Laboratory of Polytechnic of Turin.

### 5.1.4 Results of the experiment on the alginate-based heat exchanger

The test results are described in the following chapter, highlighting the variation of temperature in time and in space of the system.

From the start of the experiment corresponding to time 0s, the resistance heats the water contained in the tank and then the water is circulated by a pump into the device.

The thermal images show the adsorbent and the device support. In order to have a clear evaluation of the temperature distribution on the surface area of the device, significant points are chosen in different region and subsequently compared. In particular the centre of the squared area defining all the device is taken as benchmark. Regions on the left and on the

right are studied. The infrared images display where fins are located, so it is possible to distinguish the solid region and the fluid region. For each zone, two temperature points are chosen, one corresponding to the solid region and the other to fluid region. In addition, the software allows to capture the hottest point and the coldest point of specific areas. This kind of points changes its position in each picture, depending on the temperature variation. The reference area for the hottest point includes the whole device, instead the area where the coldest point is reached includes only the part with alginate material. For the sake of completeness, two points revealing the temperature of the support device are chosen, one in the higher part and the other in the lower part.

All references and relative nomenclature are resumed in the following table and showed in figure 2:

| Point name | Zone |
|---|---|
| M1 | Centre, centre-air |
| M2 | Centre, centre-fin |
| M3 | Left, centre-air |
| M4 | Left, centre-fin |
| M5 | Right, centre-air |
| M6 | Right, centre-fin |
| M11 | Support up |
| M13 | Support down |
| HS1 | Depend on the temperature |
| CS1 | Depend on the temperature |

**Table 17**

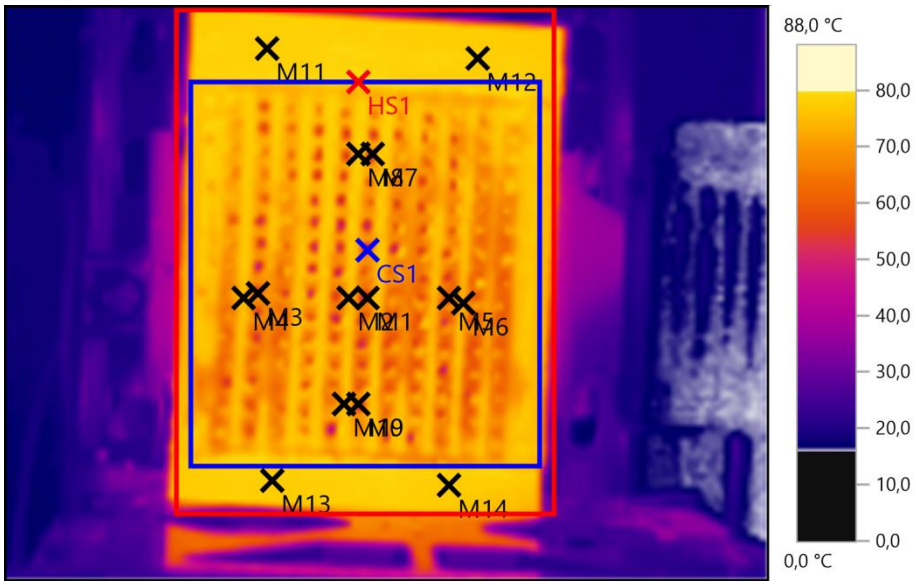


**Figure 27. Infrared image set point layout**

The temperature transient is figured in the graph 8.

From 0s to 240s images are taken with a time step of 10s. From 240s to 1500s images are taken each 30s. Different time steps are chosen in relation to the velocity of the variation of temperature in time.

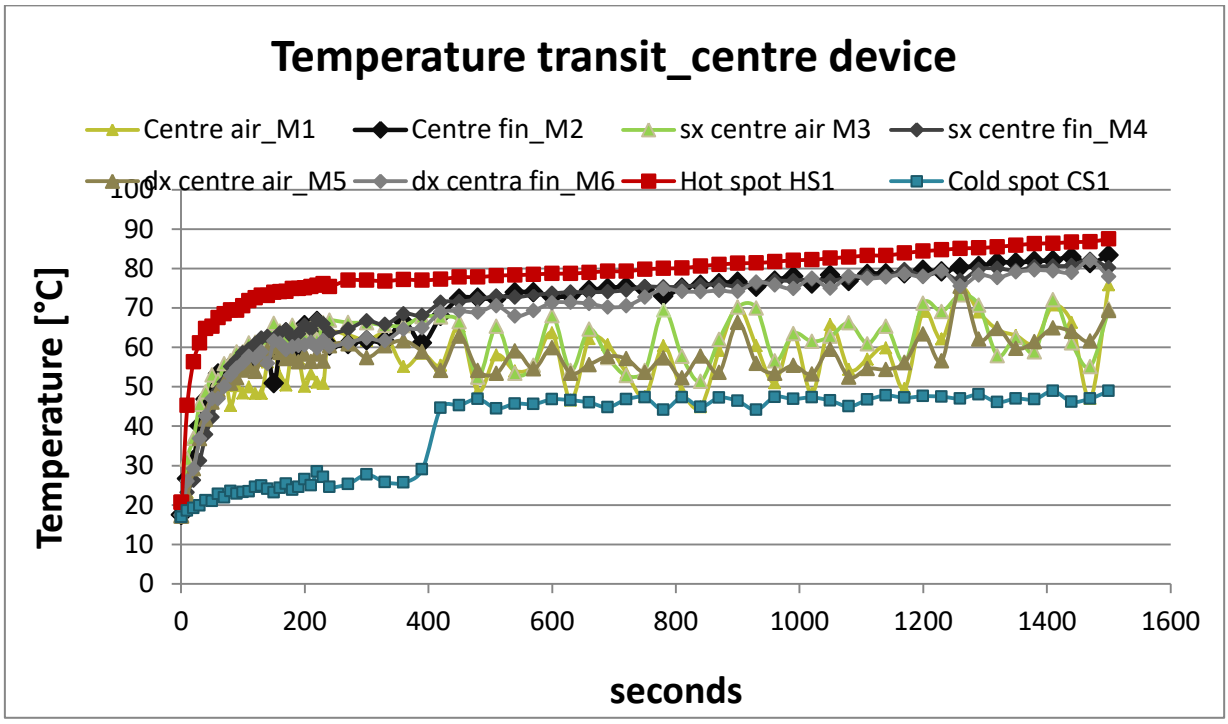


**Graph 8. Whole temperature transient of experiment of HEX**

The graph shows the dataset of the points taken in consideration. It is possible to notice two main trends: one referred to the solid region, where the fin is located, and the other one referred to the fluid region. Initially, the system heats rapidly. After about 3 minutes (180s) it reaches a plateau temperature value, that increase mostly with a linear trend. The solid region temperature trend is principally linear after a first rapid increase and is similar to the highest temperature point trend. As concern the fluid region, the temperature trend differs from the other trends. This is due to the fact that the material and the air inside the heat exchanger have thermal resistances. Indeed the air thermal conductivity is about 0.026 W/mK at ambient condition and the alginate thermal conductivity is considered equal to 0.21 W/mK, both very lower than aluminium thermal conductivity (230 W/mK). This is the reason why the fluid region can be supposed to be at lower temperature, that it is.

In addition a scattered trend can be noticed. This is because the thermal picture are made manually, so minimum movement can cause important differences on the measurements.

To resume, the temperature gradient differs between solid and fluid region, but it does not reveal significant differences between centre, left and right zones.

Infrared images at 0s,10s, 60s, 150s, 300s, 600s, 1200s and 1500s are shown:

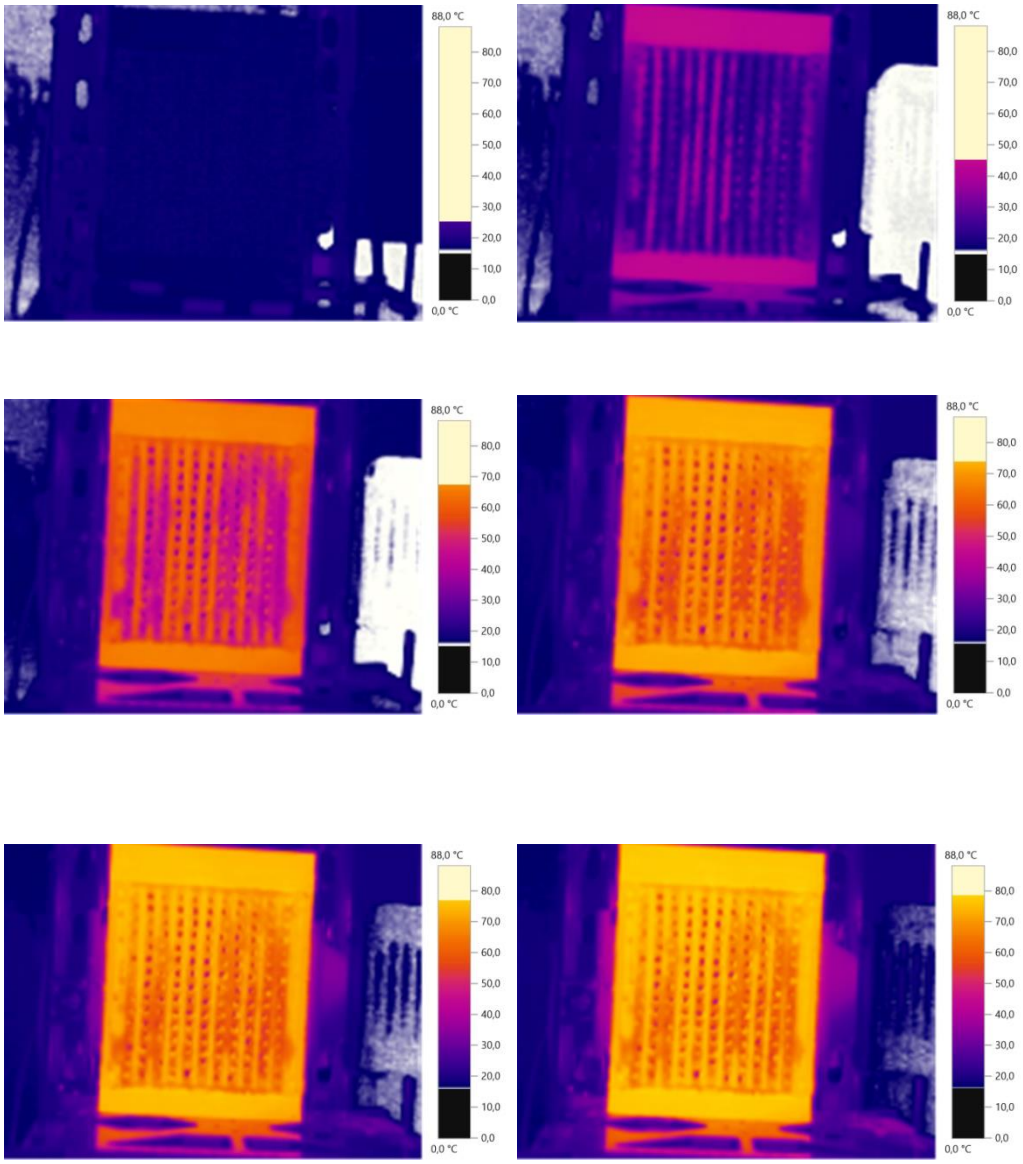

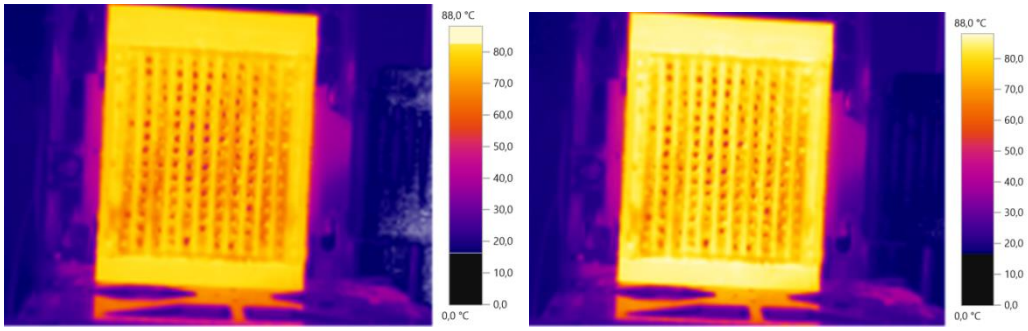


**Figure 28. Infrared images at 0s,10s, 60s, 150s, 300s, 600s, 1200s and 1500s**

The results obtained by the test conducted on the adsorbption material heated by water recirculation reveal temperature gradient variation in time: from the starting point at ambient conditions, the temperature of the material increase rapidly, but over the time a progressive smaller increases can be observed. Post-processing of infrared images allows to impose a thermal range, in order to visualize the same colour scale. In this case a scalar between 0°C and 88°C is chosen. The black band refers to the temperature range between 0°C and the minimum temperature captured, around 16°C. The white band, instead, refers to the temperature range between the maximum temperature captured in each case and the maximum temperature imposed equal to 88°C. It is clear that the end picture reaches nearly the maximum temperature imposed, and have not the white band.

Observing infrared images, at the beginning the device is at ambient temperature at 17.5°C and in 10 seconds the temperature increases until 45°C, firstly in the device support and in correspondence of the fins. After one minutes the maximum temperature registered is around 67°C, that means in 50 seconds the device heats up of 22°C. After 150 second it reaches about 75°C. A summary of the temperature ramp in the first 2.5 minutes can be showed in the graph, highlighting the difference between the alginate material temperature and the support temperatures.

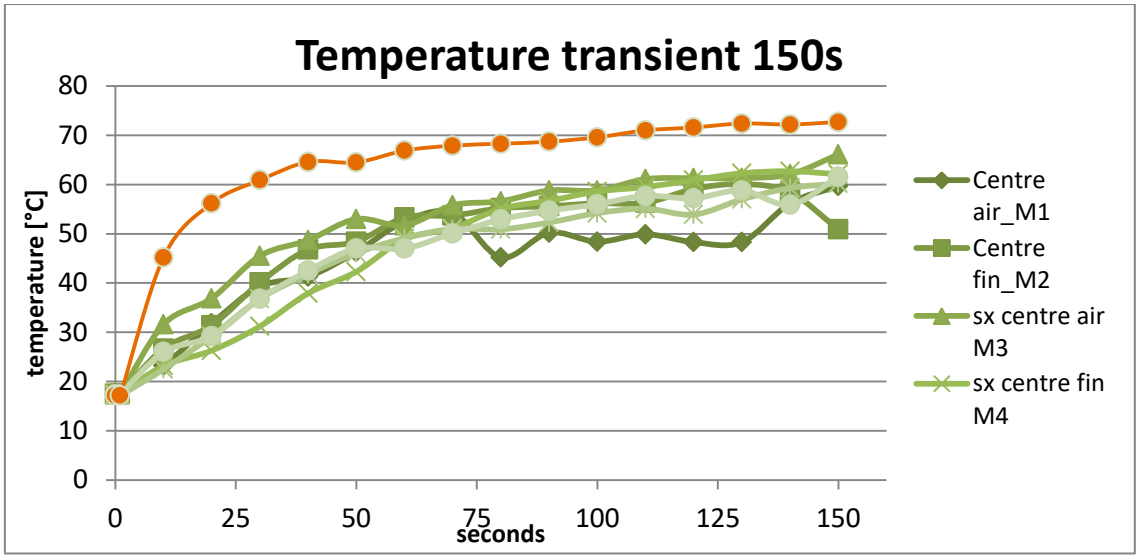


**Graph 9. temperature transient of experiment of HEX, first 2,5 minutes**

It can be noticed from thermal images that the temperature field is not uniform on the alginate area, and this may be related to the fact that the device had completed several adsorption/desorption cycle and, as consequence, the salt contained in the alginate adsorber had stuffed some areas, slowing down the heating process. This phenomenon affects the process up to 10 minutes. After 5 minutes, the temperature increase very slowly in comparison to the initial ramp. Precisely, between 5 and 10 minutes the maximum temperature increase of 3°C, and between 10 minutes and 25 minutes, it increases of 10°C, even 1°C each minutes.

The quality of the results depends on the precision of the measurements and the validity of initial assumptions. Non-metal material emissivity decreases with temperature increase, so the emissivity of the material could be lower during the test, in comparison with the initial one. In addition the surface on which the infrared sensor works is not smooth and also the roughness affects the emissivity. The thermal images are taken manually, causing an imprecision on the point of temperature evaluation.

## 5.2 Comparison with the experimental test

The best way to validate a model is by mean of a comparison between simulation solution data with experimental data.

The goal of this chapter is to verify if the temperature profile obtained by the experiment conducted on the alginate-based heat exchanger in DENERG of Polytechnic of Turin, and well explained in the previous paragraph, corresponds to the temperature profile obtained in the simulation of the heat exchanger applying the adsorption model.

The data analysis related to the experiment on the alginate-base heat exchanger is carried out and the resulting temperature profile during the whole transient is reported. As a first sight, two main trends can be noticed: one referred to the solid region, where the fin is located, and the other one referred to the air region. To make an equivalence between the geometry simulated and the geometry of the heat exchanger, the temperature profile that corresponds to the solid region is chosen.

The regeneration of the heat exchanger was performed, so the analysis has to be referred only to the regeneration phase of simulation, applying the relative initial conditions.

In the previous CFD simulations, a constant temperature is applied as *Thermal Specification* condition on the *Left* and *Right Walls* boundaries of the solid region that represents the adsorbent material. As it was expected, the temperature profile of the internal boundary, that one with hexagonal shape, tends to reach the constant temperature imposed, indication that the material is heating up during regeneration phase, realising water.

During a real regeneration cycle, the adsorbent material is heated up by hot water recirculation system, hence it undergoes a temperature transient. As consequence, the imposed condition of constant temperature does not fit anymore and has to be substituted with a realistic one, that allows to perform the variation of temperature tested on the heat exchanger.

First of all it is necessary to understand if the temperature evaluated on the solid region during the heat exchanger experiment is uniform along its geometry and if there are variation between the left zone, the centre zone or the right zone of the device tested. To do that, the thermal image at the middle of the transient is chosen as champion.

IRSoft allows to draw a line inside the area considered in the infrared image and evaluate the temperature for the number of pixels the line crosses. For this reason, three lines are drown

on what seems to be the fins position in the heat exchanger, each one for the three zone studied. The infrared image with lines is reported in figure:

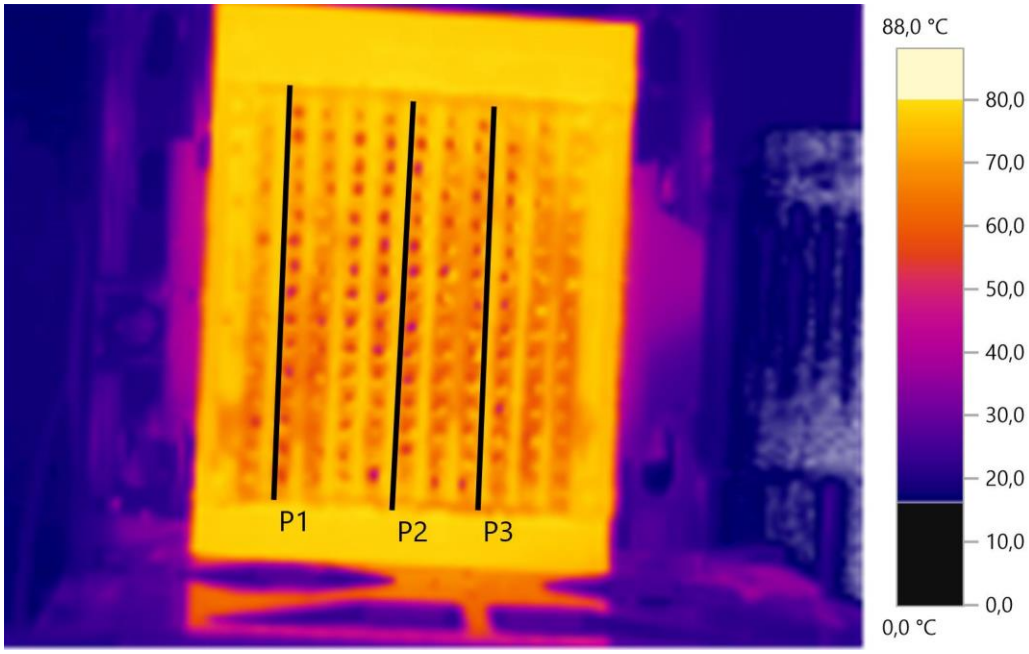


**Figure 29. Temperature Lines layout**

After that, the temperature data collected by the software are compared in order to make an analysis on the temperature distribution. The radar graph 10 shows the distributions of the three lines for 75 points. The temperature varies between a minimum of 69°C and a maximum of 78°C, with an average temperature of 75.8°C for the centre of the device, 75.79 °C for the left line and 73.95°C for the right line. From the moment that the infrared camera has a precision of ±2°C, it is clear that average values could be considered reliable. So, the distribution of temperature on the length of the fins is uniform on the adsorbent surface area, or at least on what concerns fins' positions.

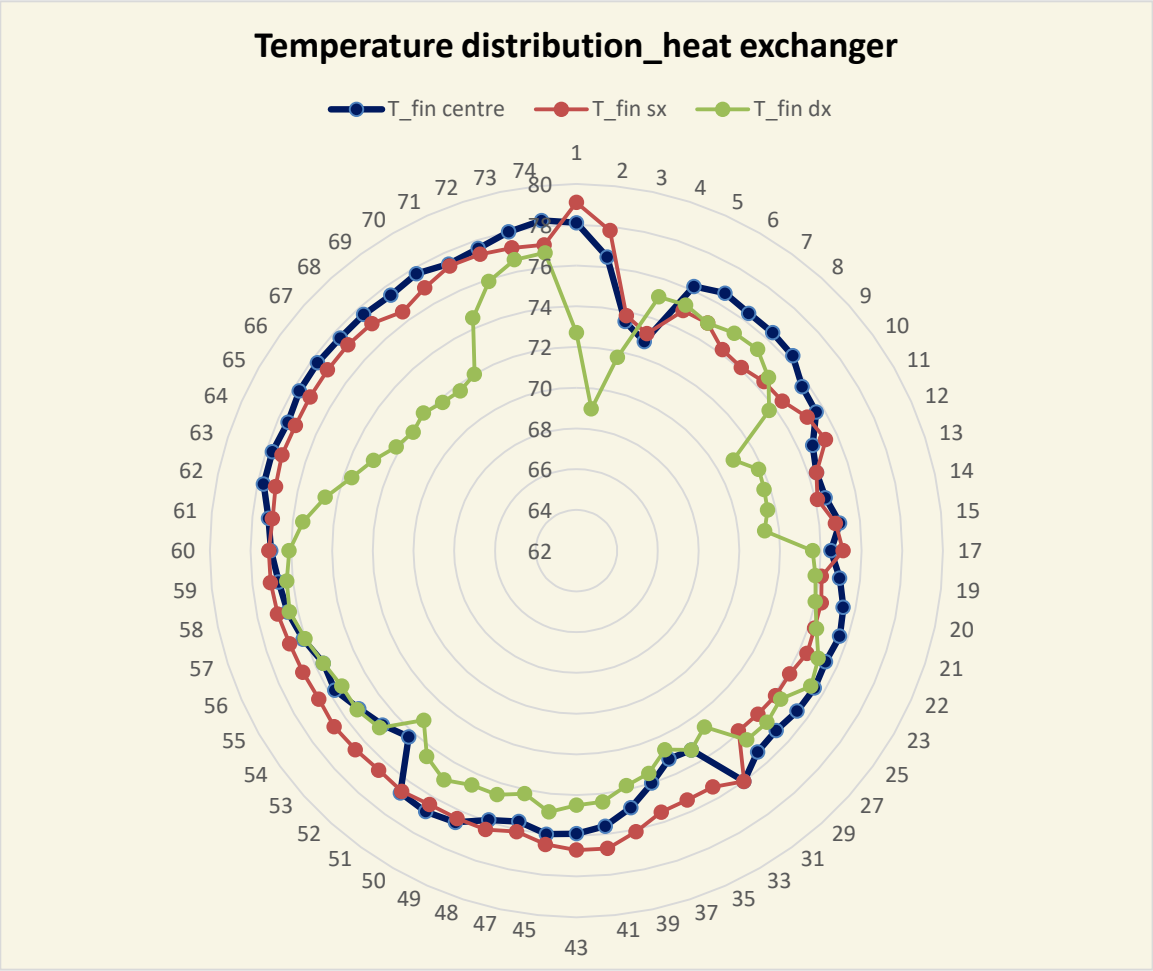


**Graph 10. Sensitivity analysis on temperature fin distribution radar graph**

The temperature distribution corresponding the centre of the device is chosen. Now, since it is impossible to perform the temperature transient for 75 points and considering that the point corresponding to the half of this distribution has a values nearly equal to the average value, the centre point is chosen (point 43). This point corresponds to the data collected during the experiment in “Centre, Centre Fin”, called M2 by the software. Its distribution is shown in the graph:

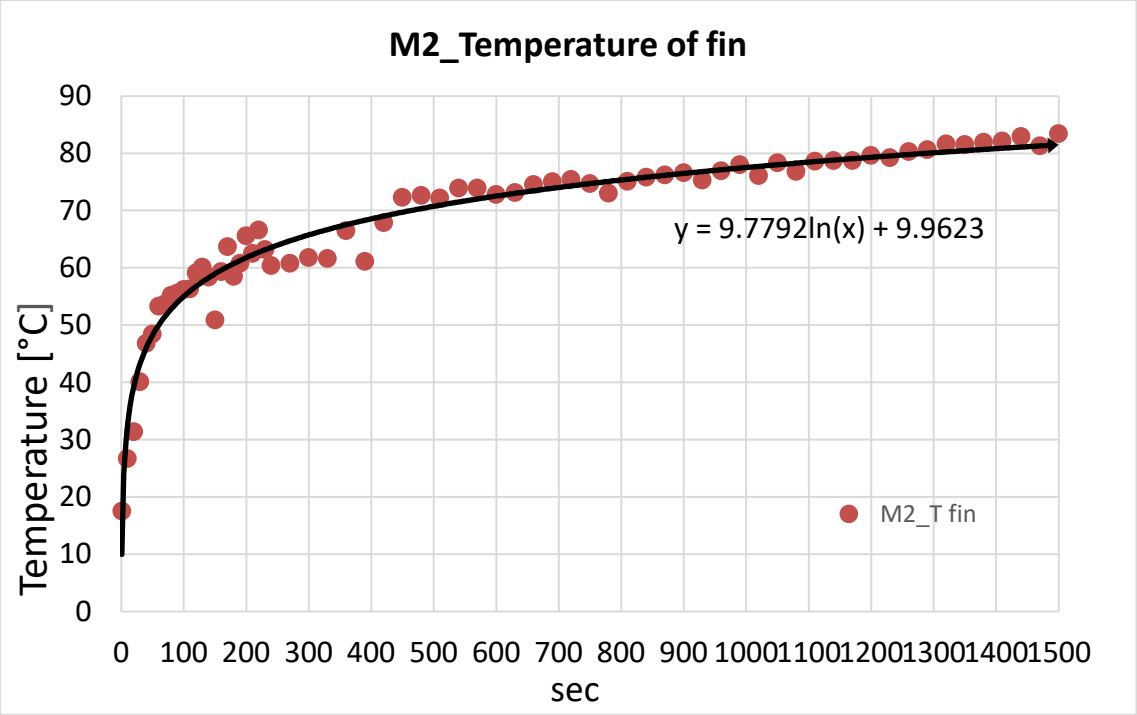


**Graph 11. Temperature Line trend for M2 fin point**

To describe the temperature variation a trend line is added: the logarithmic trend well describes the dots' disposal and it is represented by the equation displayed in the graph.

Before adding the temperature distribution, it is necessary to consider if the test experiment duration can fit the simulation time. The test lasts 1500s while, as seen in previous chapters, simulations lasts about 6000s, with a minimum of 3600s. For that reason new data points have to be found to complete the simulation transient. To do that, the logarithmic equation is used, calculating temperature each 10 seconds, and completing the transient at 3000s.

The implementation of the new data is done through *Table* tool: on the *Left* and *Right Walls* boundaries *Thermal Specification* condition is set to Temperature and the *Method* is chosen as *Table(time)*.

The result is shown in chart X. We can see that especially in the first part of the transient the curves of temperature have different inclinations, while in the second half they reach a similar trend. The experimental curve given by the data analysis of the heat exchanger test rises rapidly in comparison to the simulation one. This behaviour may be due to different aspects. First, the software recognises as input the properties of the alginate adsorbent that have a low thermal conductivity, considered to be equal to 0.21 W/mK, and solves the model on each cell of the solid. Even if the thickness of the solid region is equal to 1mm, the material has a thermal resistance and need more time to heat up and reach the input

temperature. In addition the validity of the experimental curve is related to the accuracy of the thermal imager sensor on what concerns the temperature field. The accuracy of the camera is ±2°C.

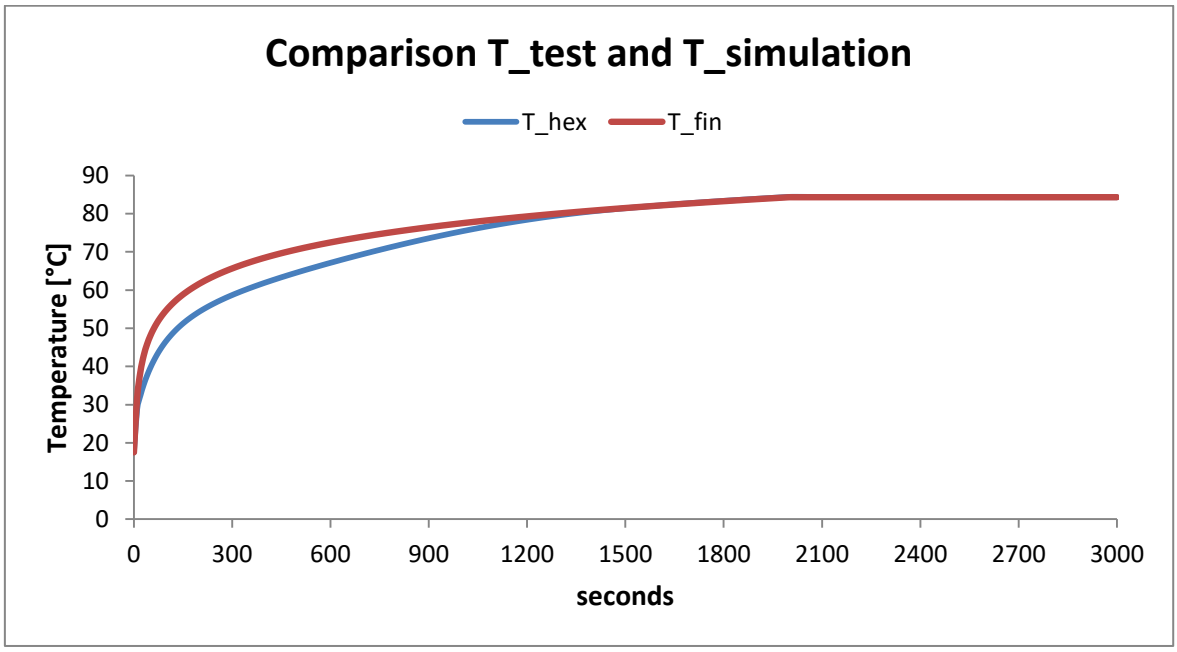


**Graph 12. Comparison between experimental temperature profile and simulated temperature profile**

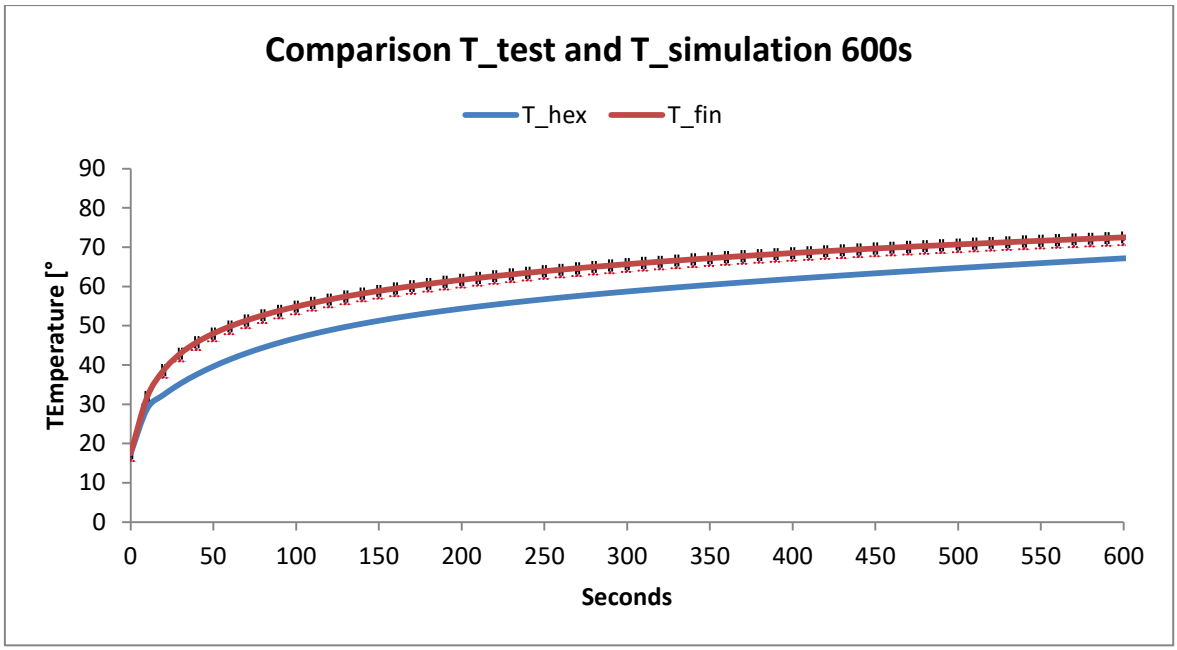


**Graph 13. Comparison between experimental temperature profile and simulated temperature profile, first 600s**

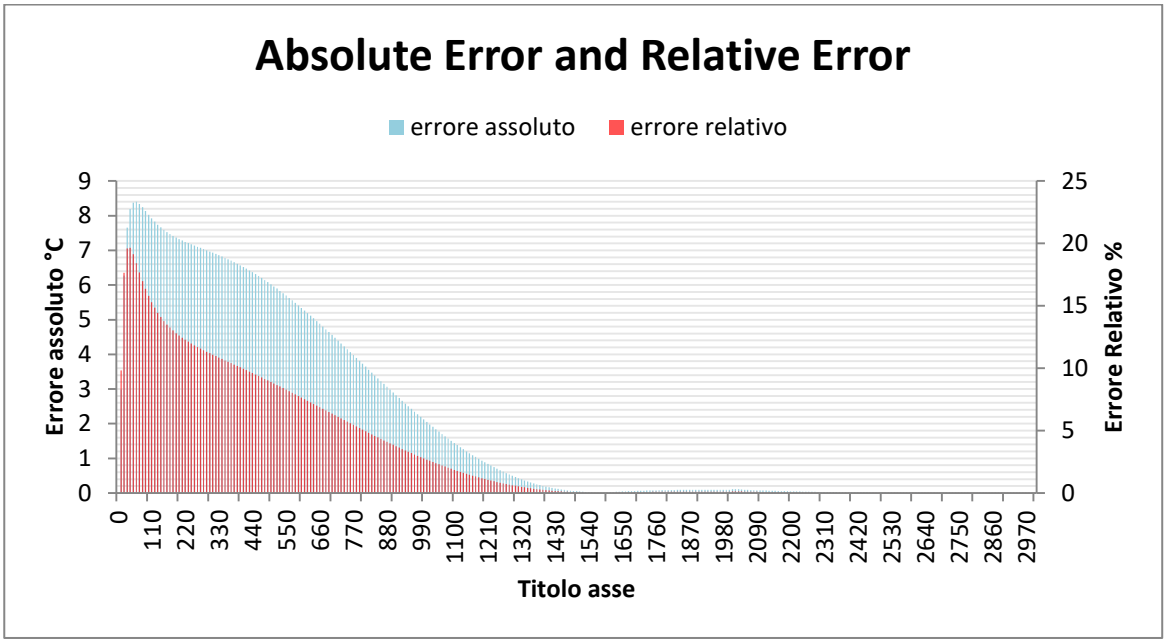


**Graph 14. Error of simulation without tolerance**

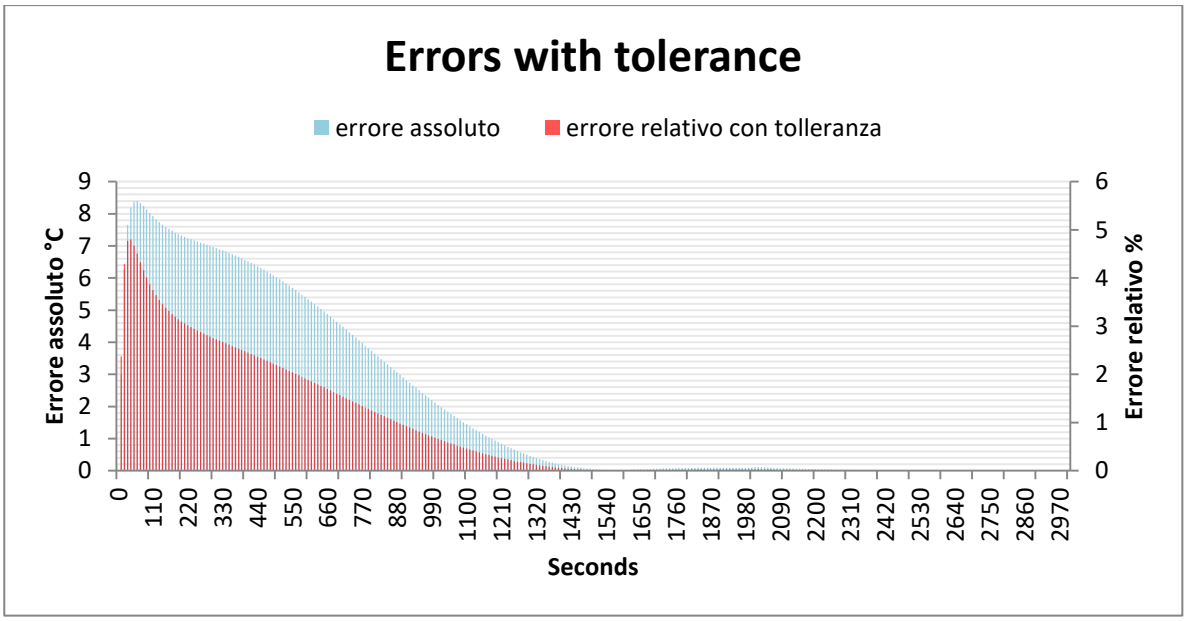


**Graph 15. Error comparison with tolerance +2°C**

The error charts show that a maximum relative error of 20% is present between the experimental temperature curve and the CFD simulation temperature curve and it is out of the range of acceptability of 10% for the first 10 minutes. Once considered the tolerance of the sensor used, the relative error falls within the 5%, that is an acceptable value.

The temperature profile influences the air moisture content and the relative humidity. To guarantee that the simulation carried out to model regeneration cycle makes sense, another evaluation of simulation results has to be done. In this respect, the air moisture content is considered. The case of regeneration with constant temperature profile of 60°C is chosen to make a comparison with that one of the transient simulation.

As shown in the graphs, the trend of both the cases are similar, but with different maximum values. This because at the beginning of the transient the temperature applied to the solid region is lower of 60°C, and so the air moisture, influenced by the temperature, increase less.

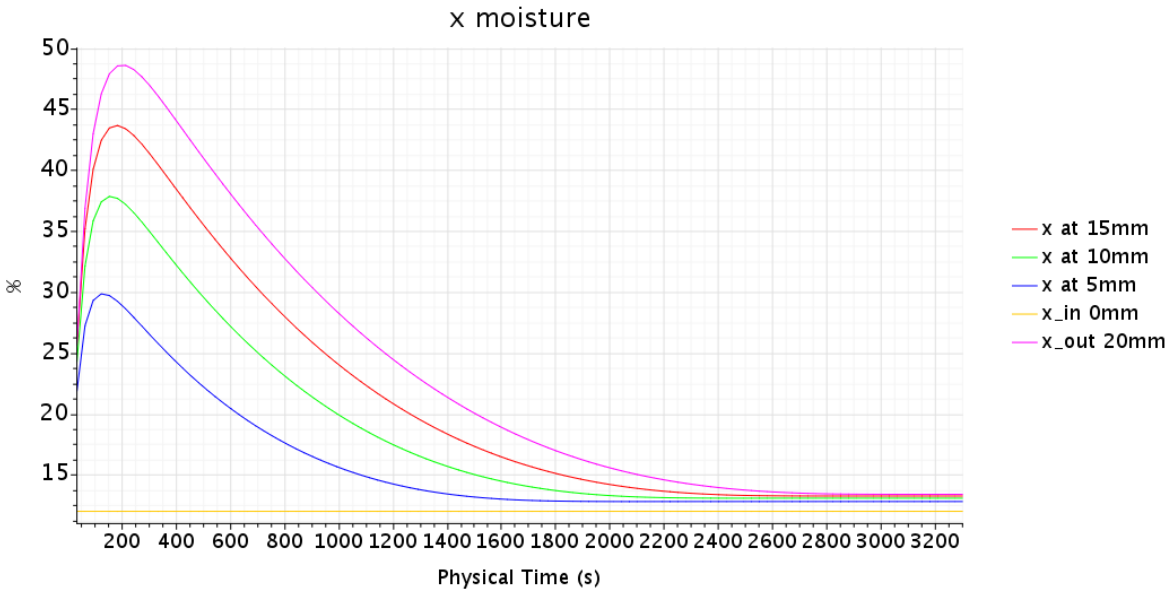


**Graph 16. Concentration of water with constant temperature profile boundary**

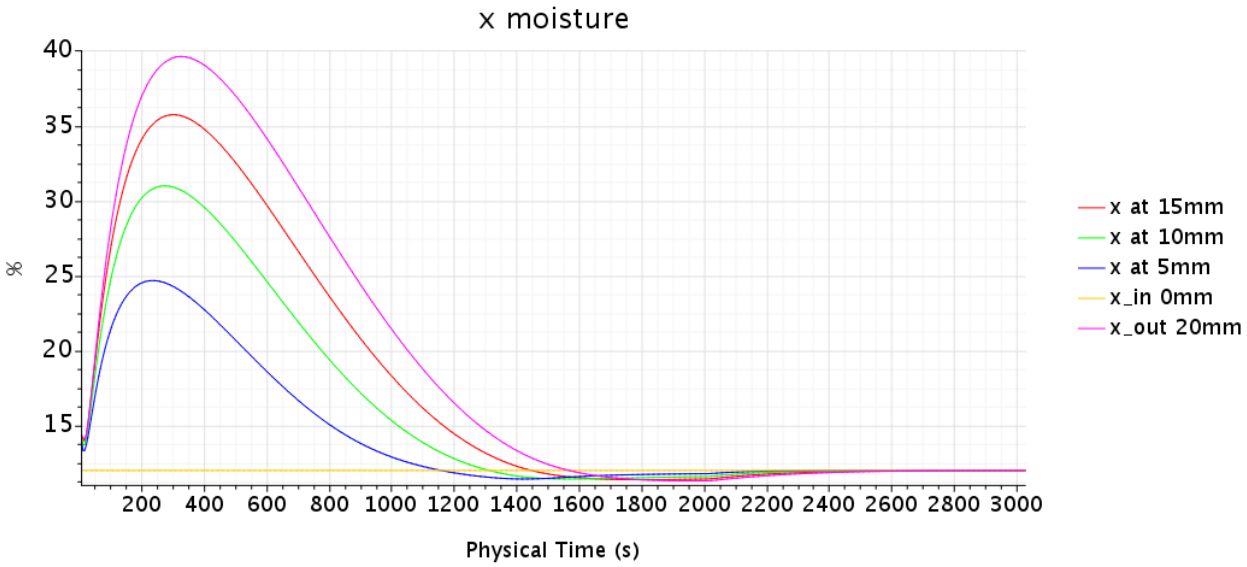


**Graph 17. Concentration of water with transient temperature profile boundary**

# Chapter 6

# Conclusions

This thesis presents a theoretical model used to simulate adsorption phenomena of water from atmospheric air in alginate-based heat exchanger.

The adsorption process is described by a CFD model that simulates the phenomenon that happens inside the heat exchanger device. The model is defined by a set of theoretical equations that make possible to describe the adsorption equilibrium on alginate-based adsorbent: heat transfer and mass transfer are evaluated simulating the model on the surface area of the adsorbent. The equations are implemented in the CFD software STAR-CCM+.

The model is thought to suit different configurations in term of geometry setting, operation conditions and in term of material properties. In the way to describe heat transfer and water adsorption from air to the adsorbent material, honeycomb configuration alginate-coated heat exchanger is chosen. To study the suitability of the model for honeycomb geometry and with alginate properties, adiabatic adsorption process is simulated. This means that the system considered is the volume air, on which no temperature condition is apply. The results show coherence between data analysed from the simulations and the experimental isotherms of alginate. In particular water uptake, relative humidity and air moisture content are compared.

In addition to the good estimation that the CFD model give to the heat exchanger adsorption phenomena, another advantage is the great reduction of time needed to simulate its work. For instance, the physical time needed for adiabatic adsorption simulation to converge is about 6 hours, while the real computational time is little more than one hour. The computational time is reduced even more carrying out a independence grid analysis on a variable of the model. The results are related to the refinement of the mesh and a balance between a good estimation of the variable considered, that is the water uptake, and the computational time is found. The mesh could be coarse without affecting the estimation of the water uptake.

The second part of this work is related to the simulation of the alginate-coated heat exchanger. An experimental test is carried out in the Energy Department of Polytechnic of

Turin in order to evaluate the temperature gradient of the alginate heat exchanger during the transient of the heating phase of regeneration process. To do that, a thermo- imagers able to capture infrared radiations is used. A sensitivity analysis shows that two main temperature fields can be distinguished: one referred to air channels and one to the adsorbent material, where fins are located. On what that concerns the solid temperature distribution, it was possible to verify that the space temperature gradient can be neglected, even if the adsorbent material has some thermal resistance during transient. Making the assumption the material has homogeneous temperature distribution, the validation of the model can be carried out implementing the temperature profile given by experiment on the heat exchanger as boundary condition. To perform that kind of simulation an extension to the model has to be added. A solid part that represents the porous adsorbent is considered and the temperature transient evaluated during the experimental test is applied as a thermal source to drive the regeneration process. The results show that the alginate adsorbent behaviour is quite different from the simulation one. In the first part of the transient a different temperature profile can be noticed. This deviation from experimental data is due to the presence of the fins, or more accurately to the fact that the experimental temperature profile is evaluated where the fins of the heat exchanger are located, while in the CFD simulation only adsorbent material is considered. So it is expected that the experimental curve increases faster than the simulated curve thanks to the high thermal conductivity of Al, mainly in the first part of the transient. That it is. Moreover the model is a simplification of the real phenomenon, so some aspects are neglected.

For these reason, considering the thermo-imager sensor tolerance of 2°C, an absolute error of around 6% can be calculated, while the relative error never exceeds 3.5%. After about 10 minutes the error decrease under 1%.

In conclusion, in future study the model can be extended towards the implementation of porous material and towards the evaluation of the velocity of diffusion of water inside the porous structure. In this study the diffusivity is considered constant, neglecting the phenomena because of its low velocity , while is well known that it is very influenced by temperature. An improvement of the model sees its application to perform other configurations and materials, maintaining low computational cost, and goes towards the investigation of new atmospheric water harvesting technologies.

.

**BIBLIOGRAFY**


[1] United Nations Educational Scientific and Cultural Organization, "LEAVING NO ONE BEHIND, The United Nations World Water Development Report 2019," 2019.

[2] "https://www.un.org/development/desa/en/." .

[3] OECD, "Environmental outlook to 2050 - key findings on biodiversity," *OECD Environ. Outlook to 2050 Consequences Ina.*, no. March, p. 7, 2012.

[4] B. Gido, E. Friedler, and D. M. Broday, "Liquid-Desiccant Vapor Separation Reduces the Energy Requirements of Atmospheric Moisture Harvesting," *Environ. Sci. Technol.*, vol. 50, no. 15, pp. 8362–8367, 2016.

[5] Y. Tu, R. Wang, Y. Zhang, and J. Wang, "Progress and Expectation of Atmospheric Water Harvesting," *Joule*, vol. 2, no. 8, pp. 1452–1475, 2018.

[6] O. Klemm *et al.*, "Fog as a fresh-water resource: Overview and perspectives," *Ambio*, vol. 41, no. 3, pp. 221–234, 2012.

[7] M. Azeem *et al.*, "Optimal Design of Multi-Layer Fog Collectors," pp. 1–34, 2020.

[8] B. Khalil *et al.*, "A review: dew water collection from radiative passive collectors to recent developments of active collectors," *Sustain. Water Resour. Manag.*, vol. 2, no. 1, pp. 71–86, Mar. 2016.

[9] A. Scrivani and U. Bardi, "A study of the use of solar concentrating plants for the atmospheric water vapour extraction from ambient air in the Middle East and Northern Africa region," *Desalination*, vol. 220(1–3), pp. 592–599.

[10] A. M. Hamed, A. A. Aly, and E.-S. B. Zeidan, "Application of Solar Energy for Recovery of Water from Atmospheric Air in Climatic Zones of Saudi Arabia," *Nat. Resour.*, vol. 02, no. 01, pp. 8–17, 2011.

[11] A. M. Hamed, "Experimental investigation on the natural absorption on the surface of sandy layer impregnated with liquid desiccant," *Renew. Energy*, vol. 28, no. 10, pp. 1587–1596, 2003.

[12] U. Bardi, "Fresh water production by means of solar concentration: the AQUASOLIS project," *Desalination*, vol. 220, no. 1–3, pp. 588–591, 2008.

[13] V. S. Nikolayev, D. Beysens, A. Gioda, I. Milimouk, E. Katiushin, and J. P. Morel, "Water recovery from dew," *J. Hydrol.*, vol. 182, no. 1–4, pp. 19–35, 1996.

[14] J. Y. Wang, R. Z. Wang, Y. D. Tu, and L. W. Wang, "Universal scalable sorption-based atmosphere water harvesting," *Energy*, vol. 165, pp. 387–395, 2018.

[15] H. Kim *et al.*, "Adsorption-based atmospheric water harvesting device for arid climates," *Nat. Commun.*, vol. 9, no. 1, pp. 1–8, 2018.

[16] J. Y. Wang, J. Y. Liu, R. Z. Wang, and L. W. Wang, "Experimental research of composite solid sorbents for fresh water production driven by solar energy," *Appl. Therm. Eng.*, vol. 121, pp. 941–950, 2017.

[17] A. Mahesh, "Solar collectors and adsorption materials aspects of cooling system.," *Renew. Sustain. Energy Rev.*, p. 1300{1312;, 2017.

[18] N. YuR.Z. WangZ. S. LuZ. S. LuL.W. WangL.W. Wang, "Development and characterization of silica gel-LiC1 composite sorbents for thermal energy storage," *Chem. Eng. Sci.*, vol. 111, pp. 73–84, 2014.

[19] G. Najeh, • Messai Souad, • Gabsi Sli, and R. Benelmirmane, "Numerical Investigation of Silica Gel-Water Solar Adsorption Cooling System with Simulink," *Am. J. Appl. Sci.*, vol. 14(8).

[20] E.C. Boelman, B.B. Saha, T. Kashiwagi, "Experimental investigation of a silica gel–water adsorption refrigeration cycle—the influence of operating conditions on cooling output and COP Part 2," *ASHRAE Trans. 101*, pp. 358–366, 1995.

[21] B. R. Ghilen Najeha, Gabsi Slimanea, Messai Souada and E. G. Mohammedb, "Performance of silica gel-water solar adsorption cooling system."

[22] K. Sukhyy, E. Belyanovskaya, Y. Kozlov, S. all 5 Authors, and M. P. Sukhyy, "Structure and adsorption properties of the composites 'silica gel–sodium sulphate', obtained by sol–gel method," • *Appl. Therm. Eng.*, vol. 64, pp. 408–412.

[23] M. V. Solovyeva, L. G. Gordeeva, T. A. Krieger, and Y. I. Aristov, "MOF-801 as a promising material for adsorption cooling: Equilibrium and dynamics of water adsorption," *Energy Convers. Manag.*, vol. 174, no. August, pp. 356–363, 2018.

[24] Y. Z. Zhang, T. He, X. J. Kong, X. L. Lv, X. Q. Wu, and J. R. Li, "Tuning Water Sorption in Highly Stable Zr(IV)-Metal-Organic Frameworks through Local Functionalization of Metal Clusters," *ACS Appl. Mater. Interfaces*, vol. 10, no. 33, pp. 27868–27874, Aug. 2018.

[25] H. Kim *et al.*, "RENEWABLE RESOURCES Water harvesting from air with metal-organic frameworks powered by natural sunlight Downloaded from," 2017.

[26] F. Fathieh, M. J. Kalmutzki, E. A. Kapustin, P. J. Waller, J. Yang, and O. M. Yaghi, "Practical water production from desert air," *Sci. Adv.*, vol. 4, no. 6, pp. 1–10, 2018.

[27] European Chemical Agency, "Zeolites classification and labelling." [Online]. Available: https://echa.europa.eu/information-on-chemicals/cl-inventory-database/-/discli/details/38124.

[28] W. P. Voo, C. W. Ooi, A. Islam, B. T. Tey, and E. S. Chan, "Calcium alginate hydrogel beads with high stiffness and extended dissolution behaviour," *Eur. Polym. J.*, vol. 75, pp. 343–353, Feb. 2016.

[29] P. Gurikov and I. Smirnova, "Non-Conventional Methods for Gelation of Alginate,"

*Gels*, vol. 4, no. 1, p. 14, Feb. 2018.

[30] K. Yamamoto, Y. Yuguchi, B. T. Stokke, P. Sikorski, and D. C. Bassett, "Local structure of Ca2+ alginate hydrogels gelled via competitive ligand exchange and measured by small angle X-ray scattering," *Gels*, vol. 5, no. 1, 2019.

[31] P. A. Kallenberger and M. Fröba, "Water harvesting from air with a hygroscopic salt in a hydrogel–derived matrix," *Commun. Chem.*, vol. 1, no. 1, p. 28, Dec. 2018.

[32] T. Andersen, P. Auk-Emblem, and M. Dornish, "3D Cell Culture in Alginate Hydrogels," *Microarrays*, vol. 4, no. 2, pp. 133–161, 2015.

[33] Jian Hua Chen Hai Tao Xing Hong XuGuoGuo PingLiWenWengShi RongHu, "Preparation, characterization and adsorption properties of a novel 3-aminopropyltriethoxysilane functionalized sodium alginate porous membrane adsorbent for Cr(III) ions."

[34] Jong-WhanRhim, "Physical and mechanical properties of water resistant sodium alginate films."

[35] N.Belhouchatab H.Zaghouane-Boudiafa César Viserasbc, "Removal of anionic and cationic dyes from aqueous solution with activated organo-bentonite/sodium alginate encapsulated beads."

[36] H. Qiu, L. Lv, B. C. Pan, Q. J. Zhang, W. M. Zhang, and Q. X. Zhang, "Critical review in adsorption kinetic models," *J. Zhejiang Univ. Sci. A*, vol. 10, no. 5, pp. 716–724, 2009.

[37] A. Freni, G. Maggio, F. Cipitì, and Y. I. Aristov, "Simulation of water sorption dynamics in adsorption chillers: One, two and four layers of loose silica grains," *Appl. Therm. Eng.*, vol. 44, pp. 69–77, Nov. 2012.

[38] R. E. Alduchov, Oleg A.; Eskridge, "Improved Magnus Form Approximation of Saturation Vapor Pressure," *J. Appl. Meteorol.*, vol. 35, no. 4, pp. 601–609.

[39] L. Calabrese, L. Bonaccorsi, P. Bruzzaniti, A. Frazzica, A. Freni, and E. Proverbio, "Adsorption performance and thermodynamic analysis of SAPO-34 silicone composite foams for adsorption heat pump applications," *Mater. Renew. Sustain. Energy*, vol. 7, no. 4, pp. 1–13, 2018.

[40] P. D. I. Torino, "Water extraction from atmospheric air : CFD model of an adsorption heat exchanger," 2018.

[41] Y. I. Aristov, M. M. Tokarev, A. Freni, I. S. Glaznev, and G. Restuccia, "Kinetics of water adsorption on silica Fuji Davison RD," *Microporous Mesoporous Mater.*, vol. 96, no. 1–3, pp. 65–71, Nov. 2006.

[42] "https://iupac.org/." .

[43] "https://it.mathworks.com/." .

[44] Siemens, "STAR-CCM+ Documentation - version 13.06," 2018.

[45] F. Moukalled, L. Mangani, and M. Darwish, *Erratum to The finite volume method in computational fluid dynamics [Fluid Mechanics and Its Applications, 113, DOI 10.1007/978-3-319-16874-6]*, vol. 113. 2016.

[46] J. H. Ferziger, M. Perić, and R. L. Street, *Computational Methods for Fluid Dynamics*. 2020.

[47] T. R. Taha, *An Introduction to Parallel Computational Fluid Dynamics*, vol. 6, no. 4. 2005.

[48] "https://thesteveportal.plm.automation.siemens.com/." .